iScience

CellPress
OPEN ACCESS

Article

The PrL^{Glu} → avBNST^{GABA} circuit rapidly modulates depression-like behaviors in male mice

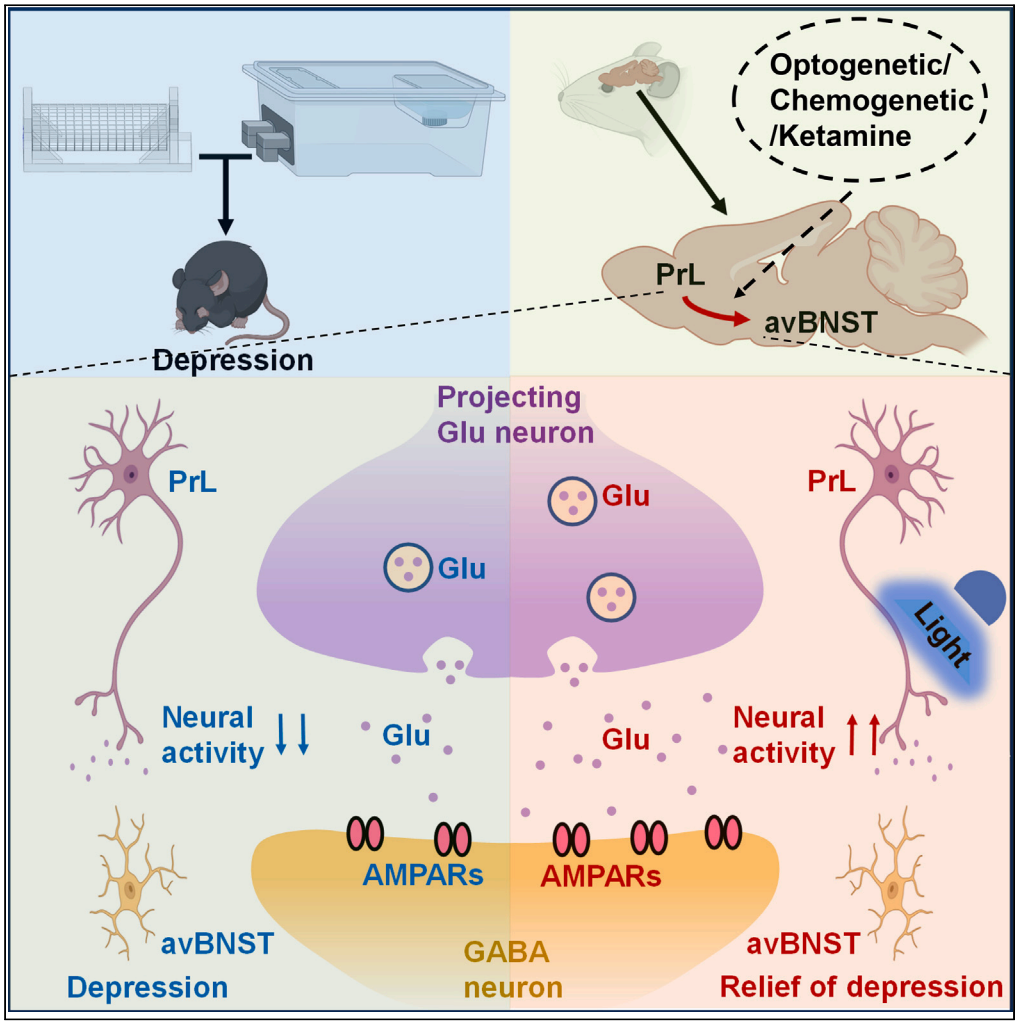

Jie-ying Chen, Ke Wu, Miao-miao Guo, Wei Song, Si-ting Huang, Yong-mei Zhang

zhangym700@163.com

Highlights

Activation of PrL^{Glu} neurons alleviated depression-like behaviors in male mice

Activation of PrL^{Glu} → avBNST^{GABA} alleviated depression-like behaviors in male mice

AMPARs played a critical role in PrL^{Glu} → avBNST^{GABA} circuit in depression

Rapid antidepressant effects of ketamine are partially mediated by PrL^{Glu} → avBNST^{GABA}

Chen et al., iScience *26*, 107878
October 20, 2023
https://doi.org/10.1016/j.isci.2023.107878

iScience

CellPress
OPEN ACCESS

Article

The PrL^{Glu} → avBNST^{GABA} circuit rapidly modulates depression-like behaviors in male mice

Jie-ying Chen,[1,2,3,5] Ke Wu,[1,2,3,5] Miao-miao Guo,[1,2,3] Wei Song,[1,2,3] Si-ting Huang,[1,2,3] and Yong-mei Zhang[1,2,3,4,6,*]

SUMMARY

Depression is a global disease with a high prevalence. Here, we examine the role of the circuit from prelimbic mPFC (PrL) to the anterior ventral bed nucleus of the stria terminalis (avBNST) in depression-like mice through behavioral tests, immunofluorescence, chemogenetics, optogenetics, pharmacology, and fiber photometry. Mice exposed to chronic restraint stress with individual housing displayed depression-like behaviors. Optogenetic or chemogenetic activation of the avBNST-projecting glutamatergic neurons in the PrL had an antidepressant effect. Moreover, we found that α-amino-3-hydroxy-5-methyl-4-isoxazole-propionicacid receptors (AMPARs) play a dominant role in this circuit. Systemic administration of ketamine profoundly alleviated depression-like behaviors in the mice and rapidly rescued the decreased activity in the PrL^{Glu} → avBNST^{GABA} circuit. Furthermore, the fast-acting effect of ketamine on depressive behaviors was diminished when the circuit was inhibited. To summarize, activating the PrL^{Glu} → avBNST^{GABA} circuit quickly ameliorated depression-like behaviors. Thus, we propose the PrL^{Glu} → avBNST^{GABA} circuit as a target for fast regulation of depression.

INTRODUCTION

Depression is a serious psychiatric disorder that is becoming increasingly prevalent.[1] Sudden depressive episodes can be difficult to manage quickly and are a high-risk factor for suicidal behavior,[2] demonstrating the need for research into rapid-acting antidepressant treatments. In spite of a growing body of work elucidating the mechanisms underlying depression, much of the underlying neurobiology is still uncertain and, as a result, the development of new clinical therapies has been extremely slow with poor outcomes.[3] For effective development of rapid-acting antidepressant therapies, it is of paramount importance that the pathogenesis of depression continues to be investigated.

Experimental and clinical studies have revealed that the central nervous system of patients with depression undergoes several changes, including the dysfunction of certain brain regions, hyperactivity of the hypothalamic–pituitary–adrenal (HPA) axis, and neurotransmitter disturbances, among others.[4–6] The medial prefrontal cortex (mPFC) is a neocortical area with diverse functions related to emotion, decision-making, social behavior and complex cognition.[7–9] It is well established that the mPFC plays a crucial role in the pathology of depression, but the specialized roles of its subregions are unclear.[10,11] The clinical therapeutic effects of mPFC-based therapies, including electroshock, transcranial magnetic stimulation, and deep-brain stimulation, are unsatisfactory[12,13] because these therapies usually result in adverse reactions such as nausea and vomiting, headaches, and even memory impairments; more precise mPFC interventions may help avoid these side effects.

The mPFC serves as a central hub that shapes the activity in a distributed network of output regions including the hippocampus, the dorsal raphe nucleus, the amygdala, and the bed nucleus of the stria terminalis (BNST),[14] with the different outputs serving different purposes. In light of this, it is necessary to explore and accurately identify the mPFC-related neural circuits involved in the regulation of depression.

The BNST receives input from multiple nuclei, including the mPFC. Because the mPFC inputs to the avBNST arise mainly from the prelimbic (PrL) subregion of the mPFC,[15] we focused on the PrL^{Glu} → avBNST^{GABA} circuit. The BNST is known as the "extended amygdala."[16] It is divided into anterior and posterior regions on the basis of neurodevelopmental and morphological differences.[17] The anterior region is linked to stress and emotion and can be further divided into the anterior medial (AM), anterior lateral (AL), and anterior ventral (AV) subregions.[18] GABAergic neurons account for more than 80% of neurons in the BNST[19] and are involved in anxiety and depression.[20] BNST GABAergic neurons regulate HPA-axis activity,[21] and our laboratory previously demonstrated that the AV subregion of the BNST plays a dominant

[1]Jiangsu Province Key Laboratory of Anesthesiology, Xuzhou Medical University, Xuzhou, Jiangsu 221002, China
[2]Jiangsu Province Key Laboratory of Anesthesia and Analgesia Application Technology, Xuzhou Medical University, Xuzhou, Jiangsu 221002, China
[3]NMPA Key Laboratory for Research and Evaluation of Narcotic and Psychotropic Drugs, Xuzhou, Jiangsu 221002, China
[4]Present address: 209 Tongshan Road, Xuzhou, Jiangsu 221002, China
[5]These authors contributed equally
[6]Lead contact
*Correspondence: zhangym700@163.com
https://doi.org/10.1016/j.isci.2023.107878

role in this.[22] HPA-axis hyperactivity is thought to be a vital mechanism of depression[23]: we thus speculated that GABAergic neurons of the avBNST may play a critical role in depression.

In recent years, depression research has focused a great deal of attention on the point of rapid antidepressant effect.[24–26] Given that, our aim in this study was to determine whether the $PrL^{Glu} \rightarrow avBNST^{GABA}$ circuit is temporally sensitive: that is, does it have a rapid modulatory effect on depressive symptoms? Ketamine is a rapid-acting antidepressant that acts much faster than fluoxetine and sertraline and is used clinically.[27] Although intolerable side effects limit its clinical application,[28] ketamine can be employed as a tool to treat depression under certain circumstances and is useful for the study of rapid anti-depressant effects. In addition, real-time *in vivo* fiber photometry can be used to quantify neocortical population activity dynamics over time.[29] Therefore, in this study, we used ketamine administration in conjunction with fiber photometry to examine the temporal sensitivity of the $PrL^{Glu} \rightarrow avBNST^{GABA}$ circuit and found that this circuit contributes to the fast modulation of depression. Our findings provide an insight into potential rapid-acting, circuit-based therapies for depression and offer a perspective on the fast antidepressant effect of ketamine at the neural-circuit level.

RESULTS

Chronic restraint stress with individual housing induces depression-like behaviors in mice

The experimental time course for model establishment and behavioral tests is depicted in Figure 1A. C57 or VGlut1-iCreERT2 male mice were assigned randomly to the control group and restraint groups. Each mouse in the restraint group was housed separately and restrained daily for 2 h in its cage. Restraint was applied between 10 a.m. and 12 p.m. on 10 consecutive days. The control group experienced 10 days of control handling. After the 10 restraint days, stress-dependent changes in mice were assessed with the open-field test, tail-suspension test, forced-swim test, and sucrose-preference test, conducted in that order. The total distance traveled in the open-field test, which was used to evaluate motor ability, did not differ between restrained mice and nonstressed control mice, or between the two strains (effect of strain ($F_{1,36}$ = 0.6303, $p > 0.05$), effect of treatment ($F_{1,36}$ = 3.718, $p > 0.05$) and effect of interaction ($F_{1,36}$ = 0.0005430, $p > 0.05$), Figure 1B). In the tail-suspension test, the groups subjected to restraint showed an increase in immobility compared with controls (effect of strain ($F_{1,36}$ = 0.9998, $p > 0.05$), effect of treatment ($F_{1,36}$ = 41.59, $p < 0.01$) and effect of interaction ($F_{1,36}$ = 1.690, $p > 0.05$), Figure 1C). In the forced-swim test, the restraint groups experienced longer periods of immobility than the control groups (effect of strain ($F_{1,36}$ = 1.765, $p > 0.05$), effect of treatment ($F_{1,36}$ = 27.42, $p < 0.01$) and effect of interaction ($F_{1,36}$ = 0.01010, $p > 0.05$), Figure 1D). In the sucrose-preference assay, sucrose consumption at 2 h was reduced in the restraint groups compared with the control groups (effect of strain ($F_{1,36}$ = 11.20, $p < 0.01$), effect of treatment ($F_{1,36}$ = 87.75, $p < 0.01$) and effect of interaction ($F_{1,36}$ = 0.001878, $p > 0.05$), Figure 1E). These results indicate that chronic restraint stress with individual housing induces depression-like behaviors in male mice.

To investigate whether female mice experiencing chronic restraint stress with individual housing develop depressive-like behaviors like males, we also recruited female C57 mice (Figure 1F). In the open-field test, there was no difference in the total movement distance between control and restraint groups, demonstrating similar motor abilities (t_{18} = 0.273, $p > 0.05$, Figure 1G). Similarly, no significant differences were observed between the two groups in the tail-suspension, forced-swim, and sucrose-preference tests (t_{18} = 0.8275, $p > 0.05$, Figure 1H; t_{18} = 0.3564, $p > 0.05$; Figure 1I; t_{18} = 1.119, $p > 0.05$; Figure 1J). In summary, chronic restraint stress with individual housing did not lead to depression-like behaviors in female mice.

Reduced activity in prelimbic mPFC glutamatergic neurons after chronic restraint stress with individual housing

To identify brain regions with altered activity during depression, we examined c-Fos expression in several regions associated with depression (Figure 2A). We detected changes in the level of c-Fos protein in the anterior cingulate cortex (ACC), PrL (Figure 2C), avBNST, alBNST, the paraventricular nucleus of the hypothalamus (PVN), and the lateral habenula (LHb) (ACC, t_{10} = 4.68, $p < 0.01$; PrL, t_{10} = 3.43, $p < 0.01$; avBNST, t_{10} = 4.871, $p < 0.01$; alBNST, t_{10} = 2.311, $p < 0.05$; PVN, t_{10} = 4.214, $p < 0.01$; LHb, t_{10} = 4.722, $p < 0.01$; Figure 2B). Moreover, we compared the density of c-Fos in these brain regions (ACC, t_{10} = 4.677, $p < 0.01$; PrL, t_{10} = 3.424, $p < 0.01$; avBNST, t_{10} = 4.855, $p < 0.01$; alBNST, t_{10} = 2.31, $p < 0.05$; PVN, t_{10} = 4.213, $p < 0.01$; LHb, t_{10} = 4.722, $p < 0.01$; Figure 2B). Among these regions, the PrL and avBNST both showed a clear decrease in the number of c-Fos-positive cells in the restraint group compared with the control group.

To further investigate the changes in neuronal activity in the PrL after chronic restraint stress with individual housing, we performed immunofluorescence staining for c-Fos, CaMKIIα (calcium/calmodulin-dependent protein kinase type II, α subunit, a marker of glutamatergic neurons), and GAD1 (glutamate decarboxylase 1, a marker of GABAergic neurons) (Figure 2E). PrL sections were prepared from control- or restraint-group mice after the 10 days of restraint. Fluorescence images show a decrease in the number of c-Fos-positive cells co-labeled with CaMKIIα in the restraint group compared with the control group (t_{10} = 5.121, $p < 0.01$, Figure 2D), whereas there was no significant difference in the number of c-Fos-positive cells co-labeled with GAD1 in the PrL (t_{10} = 0.846, $p > 0.05$, Figure 2D). This indicates that the activity of glutamatergic neurons in the PrL is reduced when mice are in a depressive state induced by chronic restraint stress with individual housing.

To further evaluate this decrease in activity of glutamatergic neurons in the PrL, we performed fiber photometry in VGlut1-iCreERT2 mice. The VGlut1 subtype is the predominant sybtype of glutamatergic neuron in the cerebral cortex. We injected rAAV-Ef1α-DIO-GCaMp6s-WPRE-hGH-pA into the PrL of VGlut1-iCreERT2 mice to express the Cre-dependent GCaMP6s calcium indicator specifically in glutamatergic cells, and examined changes in GCaMP6s fluorescence signal through an optical fiber located in the PrL (Figure 2G). We combined fiber photometry recordings with the tail-suspension test and measured changes in GCaMP6s fluorescence intensity in mice before (baseline) (Figure 2H) and after (Figure 2I) 10 days of chronic restraint stress with individual housing (restraint). The resulting traces reflect the ensemble

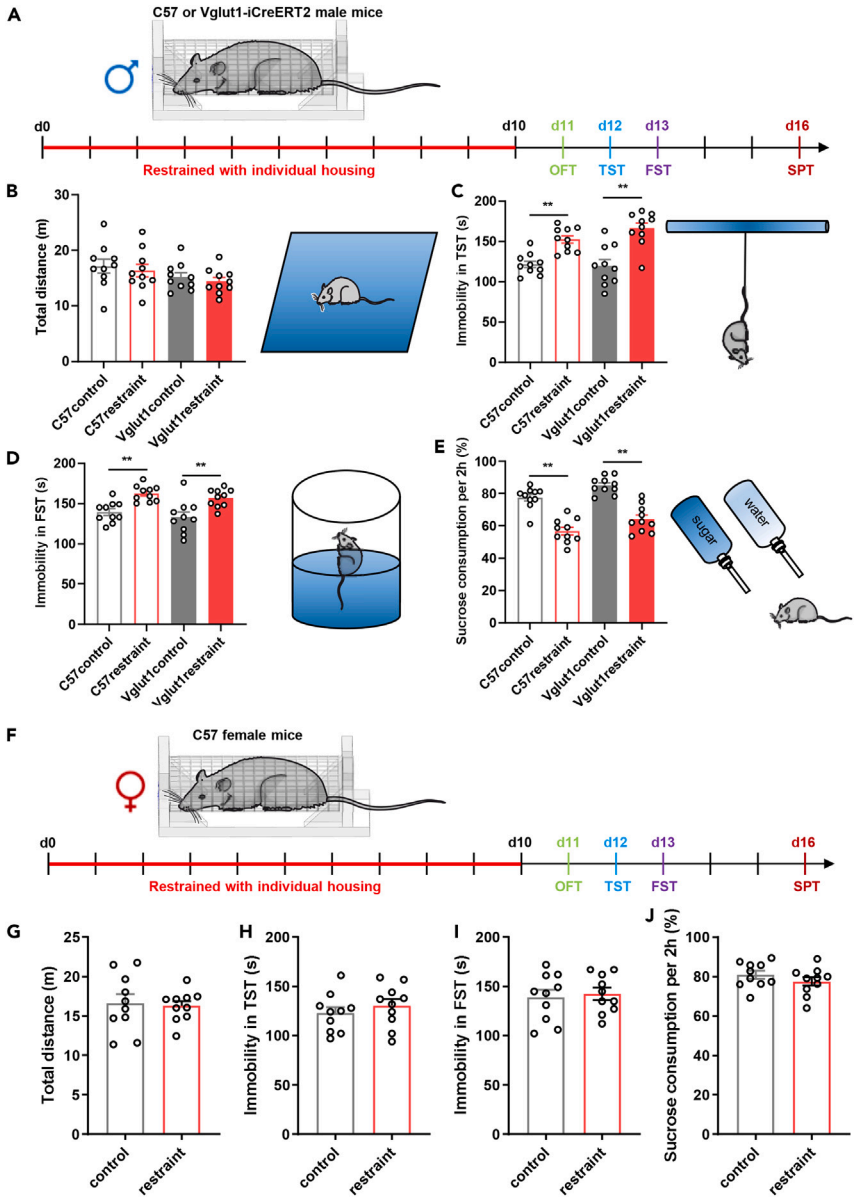

Figure 1. Chronic restraint stress with individual housing induces depression-like behaviors in mice

(A) Experimental time course (OFT, open-field test; TST, tail-suspension test; FST, forced-swim test; SPT, sucrose-preference test) of C57 or VGlut1-iCreERT2 male mice.

(B) No difference in total distance traveled in the open-field test between control and restraint groups for both wild-type (C57) and VGlut1-iCreERT2 mice (n = 10 mice per group, $p > 0.05$, two-way ANOVA and Bonferroni post hoc tests).

(C) In the tail-suspension task, the duration of immobility was higher in the restraint group than in the control group for both wild-type (C57) and VGlut1-iCreERT2 mice. There was no difference between two strains (n = 10 mice per group, $^{**}p < 0.01$, two-way ANOVA and Bonferroni post hoc tests).

(D) In the forced-swim test, the duration of immobility was higher in the restraint group than in the control group for both C57 and VGlut1-iCreERT2 mice. There was no difference between two strains (n = 10 mice per group, $^{**}p < 0.01$, two-way ANOVA and Bonferroni post hoc tests).

(E) Sucrose consumption in 2 h was reduced in the restraint group compared with the control group, for both C57 and VGlut1-iCreERT2 mice (n = 10 mice per group, $^{**}p < 0.01$, two-way ANOVA and Bonferroni post hoc tests).

(F) Experimental time course of C57 female mice.

(G–J) No difference among the control and restraint groups for C57 female mice in the open-field test, tail-suspension test, forced-swim test and sucrose-preference test (n = 10 mice per group, $p > 0.05$, two-tailed student's t-tests). Data are represented as mean ± SEM.

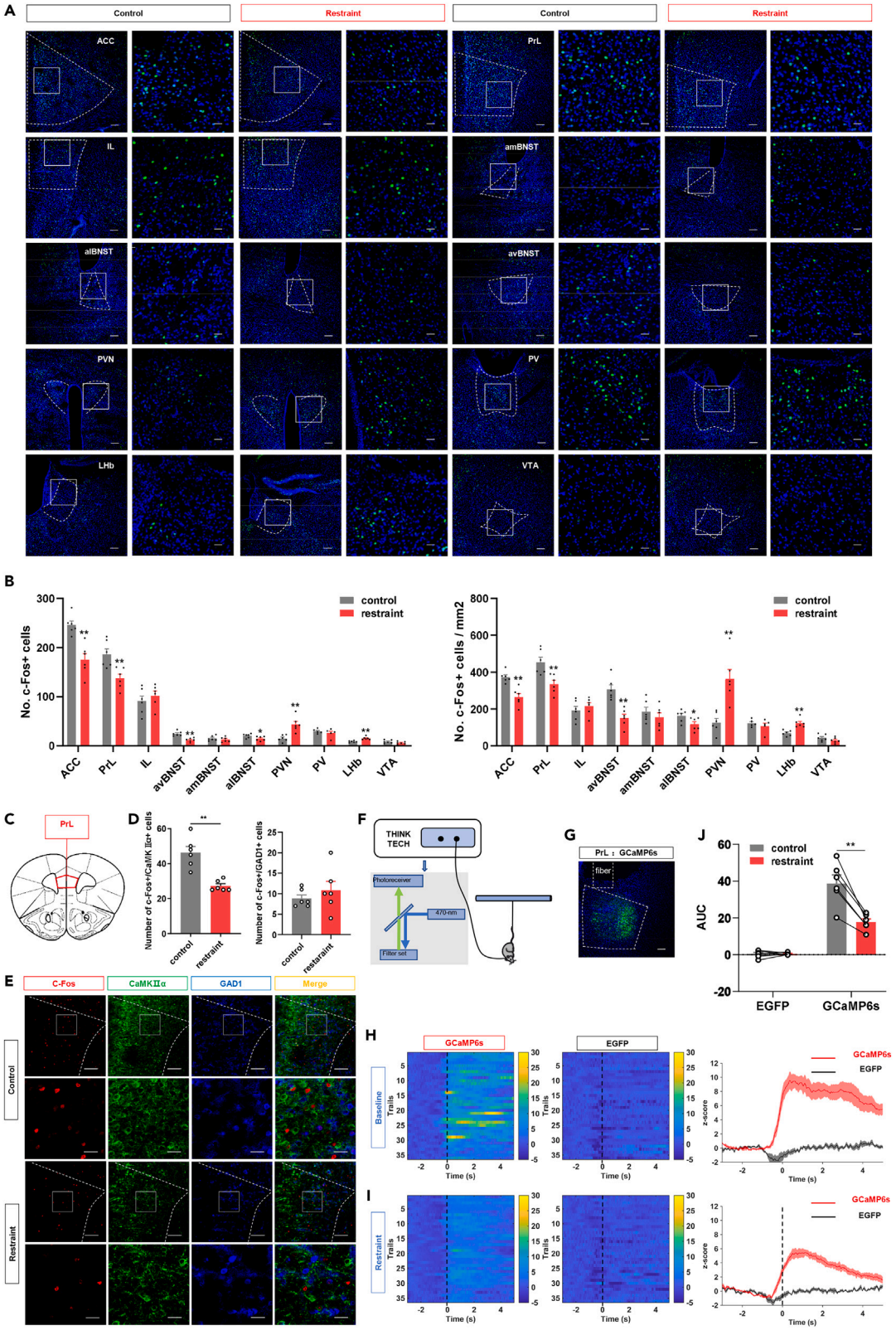
A
Control
Restraint
Control
Restraint
ACC
PrL
IL
amBNST
alBNST
avBNST
PVN
PV
LHb
VTA
B
control
restraint
No. c-Fos+ cells
No. c-Fos+ cells / mm2
ACC
PrL
IL
avBNST
amBNST
alBNST
PVN
PV
LHb
VTA
C
PrL
D
Number of c-Fos+/CaMK IIα+ cells
Number of c-Fos+/GAD1+ cells
control
restraint
E
C-Fos
CaMKIIα
GAD1
Merge
Control
Restraint
F
THINK TECH
Photoreceiver
470-nm
Filter set
G
PrL : GCaMP6s
fiber
J
control
restraint
AUC
EGFP
GCaMP6s
H
GCaMP6s
EGFP
Baseline
Trails
Time (s)
z-score
I
Restraint

Figure 2. Reduced activity in PrL glutamatergic neurons after chronic restraint stress with individual housing

(A) Representative fluorescence images of c-Fos+ cells in the ACC, PrL, IL, amBNST, alBNST, avBNST, PVN, PV, LHb, VTA. The scale bar = 100 μm. (ACC, anterior cingulate cortex; PrL, prelimbic mPFC; IL, infralimbic mPFC; amBNST, anterior medial bed nucleus of the stria terminalis; alBNST, anterior lateral bed nucleus of the stria terminalis; avBNST, anterior ventral bed nucleus of the stria terminalis; PVN, paraventricular nucleus of hypothalamus; PV, paraventricular thalamic nucleus; LHb, lateral habenula; VTA, ventral tegmental area). First, third, fifth and seventh columns, scale bars = 100 μm. Second, fourth, sixth and eighth columns, scale bars = 25 μm.

(B) Left: The number of c-Fos+ cells in the restraint group compared with the control group in left brain regions (n = 6 mice per group, *$p < 0.05$, **$p < 0.01$, two-tailed student's t-tests). Right: The number of c-Fos+ cells per square millimetre in the restraint group compared with the control group in left brain regions (n = 6 mice per group, *$p < 0.05$, **$p < 0.01$, two-tailed student's t-tests).

(C) Schematic diagram of a coronal section through PrL.

(D) The number of c-Fos+ cells co-labeled with the glutamatergic neuronal marker CaMKIIα (n = 6 mice per group, **$p < 0.01$, two-tailed student's t-tests) or with the GABAergic neuronal marker GAD1 (n = 6 mice per group, $p > 0.05$, two-tailed student's t-tests) in control and restraint groups.

(E) Representative fluorescence images of c-Fos+ cells co-labeled CaMKIIα or GAD1 in the PrL. First and third row, scale bars = 100 μm. Second and fourth rows, scale bars = 25 μm.

(F) Diagram of the fiber-photometry system.

(G) Fluorescence image of GCaMP6s expressed in PrL. Scale bar = 100 μm.

(H) Left and middle: Heatmaps of Ca^{2+} signals time-locked to the initiation of struggling in the baseline group (left: GCaMP6s; middle: EGFP control). Right: averaged struggle-locked Ca^{2+} transients for the two groups. Solid lines indicate the mean, shaded areas represent the SEM.

(I) Same as panel h but for the restraint group.

(J) Summary of area-under-the-curve (AUC) Ca^{2+} data from the struggle-locked trials (n = 6 mice per group, **$p < 0.01$, two-way ANOVA and Bonferroni post hoc tests). Data are represented as mean ± SEM.

activity of glutamatergic neurons in the PrL (Figures 2H and 2I). Mice injected with control virus (EGFP) exhibited a negligible change in fluorescence intensity under the same conditions, demonstrating that the recorded changes in *Z* score were not movement artifacts (Figures 2H and 2I). Our analysis of the time-locked areas under the calcium-signaling curves (AUCs) showed that the AUC value diminished after chronic restraint stress with individual housing (effect of virus ($F_{1,20} = 121$, $p < 0.01$), effect of treatment ($F_{1,20} = 17.16$, $p < 0.01$) and effect of interaction ($F_{1,20} = 17.26$, $p < 0.01$), Figure 2J). And, this change was not caused by repeating the tail-suspension test (Figure S1). These results confirm that the activity of glutamatergic neurons in mouse PrL is reduced after chronic restraint stress with individual housing.

Chemogenetic activation and inhibition of prelimbic mPFC glutamatergic neurons regulates depression-like behaviors

Next, we used chemogenetic manipulation of PrL glutamatergic neurons to examine their role in depression-like behaviors. First, for chemogenetic inhibition, we injected rAAV-Ef1α-DIO-hM4D(Gi)-mCherry-WPRE-pA or rAAV-Ef1α-DIO-mCherry-WPRE-pA (control virus) into bilateral PrL in naive VGlut1-iCreERT2 mice that had not undergone the restraint paradigm; Figure 3A illustrates the timeline of the experiment. Both groups of mice received intraperitoneal injection of CNO (3 mg/kg) or saline 30 min before the behavioral tests. In the open-field test, there was no significant difference in the total movement distance between groups, demonstrating similar motor abilities ($F_{2,\ 21} = 1.362$, $p > 0.05$, Figure 3B). However, in the tail-suspension test, mice in the CNO+hM4D group had more immobility time compared with the CNO+mCherry or saline+hM4D group ($F_{2,\ 21} = 4.337$, $p < 0.05$, Figure 3C); similarly, in the forced-swim test, the CNO+hM4D group had a more prolonged immobile time in the water compared with the CNO+mCherry or saline+hM4D group ($F_{2,\ 21} = 4.302$, $p < 0.05$, Figure 3D). In the sucrose-preference test, mice in the CNO+hM4D group had consumed less sugar water after 2 h than mice in the CNO+mCherry or saline+hM4D group ($F_{2,\ 21} = 21.17$, $p < 0.01$, Figure 3E). These results demonstrate that the chemogenetic inhibition of PrL glutamatergic neurons induces depression-like behaviors in naive mice.

Next, we tested whether the chemogenetic activation of PrL glutamatergic neurons alleviates depression-like behavior in mice that have undergone the restraint-stress paradigm. We injected rAAV-Ef1α-DIO-hM3D(Gq)-mCherry-WPRE-pA or rAAV-Ef1α-DIO-mCherry-WPRE-pA into bilateral PrL in VGlut1-iCreERT2 mice, as shown in Figure 3F; behavioral tests were conducted after the 10-day period of chronic restraint stress with individual housing. All groups of mice received intraperitoneal injection of CNO (3 mg/kg) or saline 30 min before the behavioral tests. In the open-field test, there were no obvious differences between groups in the total distance traveled ($F_{2,\ 21} = 0.7607$, $p > 0.05$, Figure 3G). However, remission of depression-like behaviors with chemogenetic PrL^{Glu} activation was reflected in reduced immobility times in the tail-suspension test ($F_{2,\ 21} = 7.455$, $p < 0.01$, Figure 3H) and forced-swim test ($F_{2,\ 21} = 4.502$, $p < 0.05$, Figure 3I). Of note, in the sucrose-preference test, consumption of sugar water after 2 h was higher in the CNO+hM3D group than in the CNO+mCherry or saline+ hM3D group ($F_{2,\ 21} = 12.66$, $p < 0.01$, Figure 3J). These results indicate that the chemogenetic activation of PrL glutamatergic neurons has an antidepressant effect.

Glutamatergic prelimbic mPFC neurons project to GABAergic neurons in the anterior ventral bed nucleus of the stria terminalis

The PrL sends projections to several brain regions, including the avBNST. As a preliminary step toward more accurate mapping of the glutamatergic projections, we injected rAAV-Ef1α-DIO-EGFP into the PrL in VGlut1-iCreERT2 mice (Figure 4A) and observed prominent EGFP+ fibers in the avBNST, caudate putamen (CPu), shell of the nucleus accumbens (AcbSh), claustrum (Cl), ventral pallidum (VP), zona incerta (ZI), lateral habenular nucleus (LHb), basolateral amygdaloid nucleus (BLA), and pontine nuclei (Pn) eight weeks later (Figure 4B). The target regions for the PrL glutamatergic output include sensory, autonomic, and motor structures, as well as structures involved in the processing of

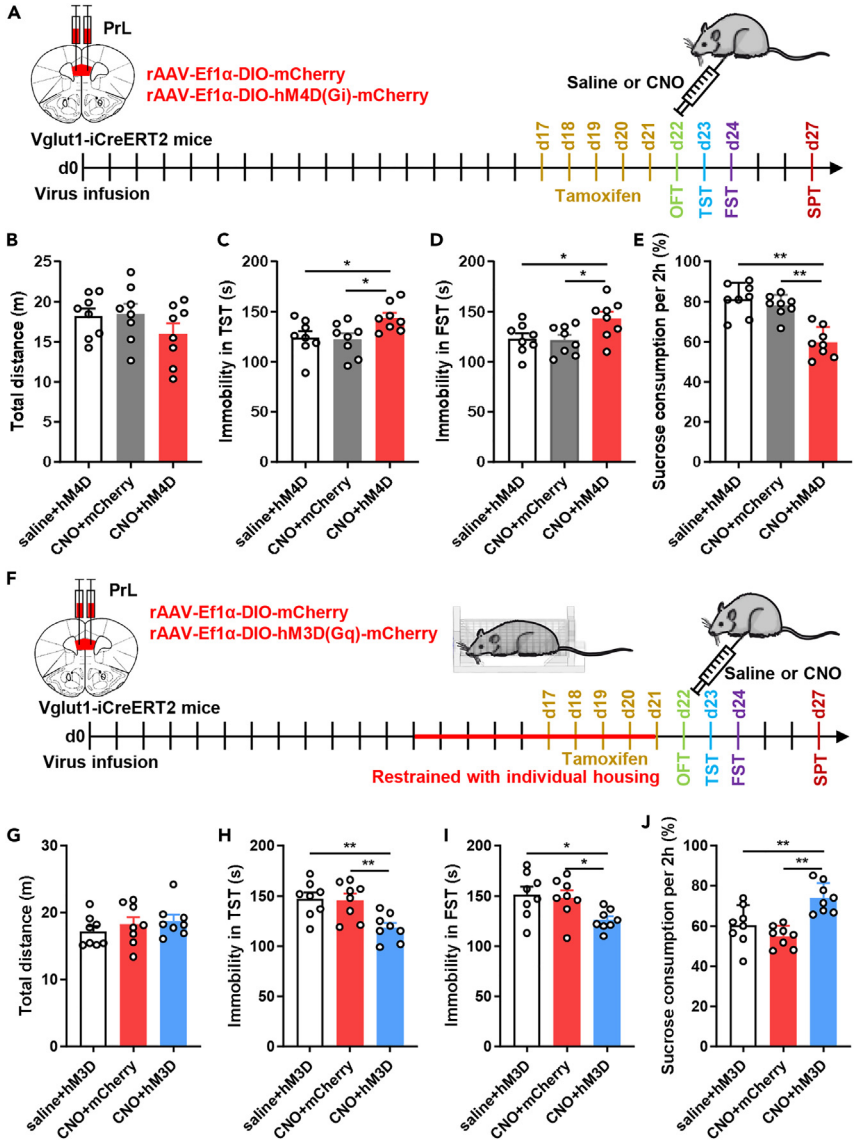

Figure 3. Glutamatergic PrL neurons are involved in depression-like behaviors

(A) Time course of the chemogenetic inhibition experiment.

(B–E) Comparison of behavior in the open-field test, tail-suspension test, forced-swim test and sucrose-preference test between saline+hM4D, CNO+mCherry and CNO+hM4D groups (n = 8 mice per group, *p < 0.05, **p < 0.01, one-way ANOVA and Bonferroni post hoc tests).

(F) Time course of the chemogenetic activation experiment.

(G–J) Comparison of behavior in the open-field test, tail-suspension test, forced-swim test and sucrose-preference test between saline+hM3D, CNO+mCherry and CNO+hM3D groups (n = 8 mice per group, *p < 0.05, **p < 0.01, one-way ANOVA and Bonferroni post hoc tests). Data are represented as mean ± SEM.

aversive and rewarding stimuli. This heterogeneity may underlie the PrL responses to diverse stimuli and states. On the basis of our previous findings regarding the contribution of the avBNST to HPA axis activity, we decided to focus on the PrL–avBNST circuit.[22] We injected rAAV-CAG-DIO-WGA-FLP into the PrL and rAAV-Ef1α-fDIO-EGFP into the avBNST in VGlut1-iCreERT2 mice (Figure 4C), to map transsynaptic transmission from PrL glutamatergic neurons to the avBNST. Immunostaining for GAD1 indicated that GABAergic neurons are the main target of PrL^{Glu} projections to the avBNST (Figures 4D and 4E).

To confirm the structural association between the PrL and the avBNST, we injected the circuit-specific retrograde virus rAAV-Ef1α-DIO-mCherry-WPRE-pA into the avBNST to identify upstream nuclei (Figure 4F). Four weeks after injection, we observed abundant expression of mCherry in PrL layer V (Figures 4G and 4H), which is consistent with observations of elevated activity in layer V mPFC pyramidal neurons after ketamine administration.[30] Together, the results from our viral tracing experiments demonstrate that glutamatergic neurons in the PrL project to GABAergic neurons in the avBNST.

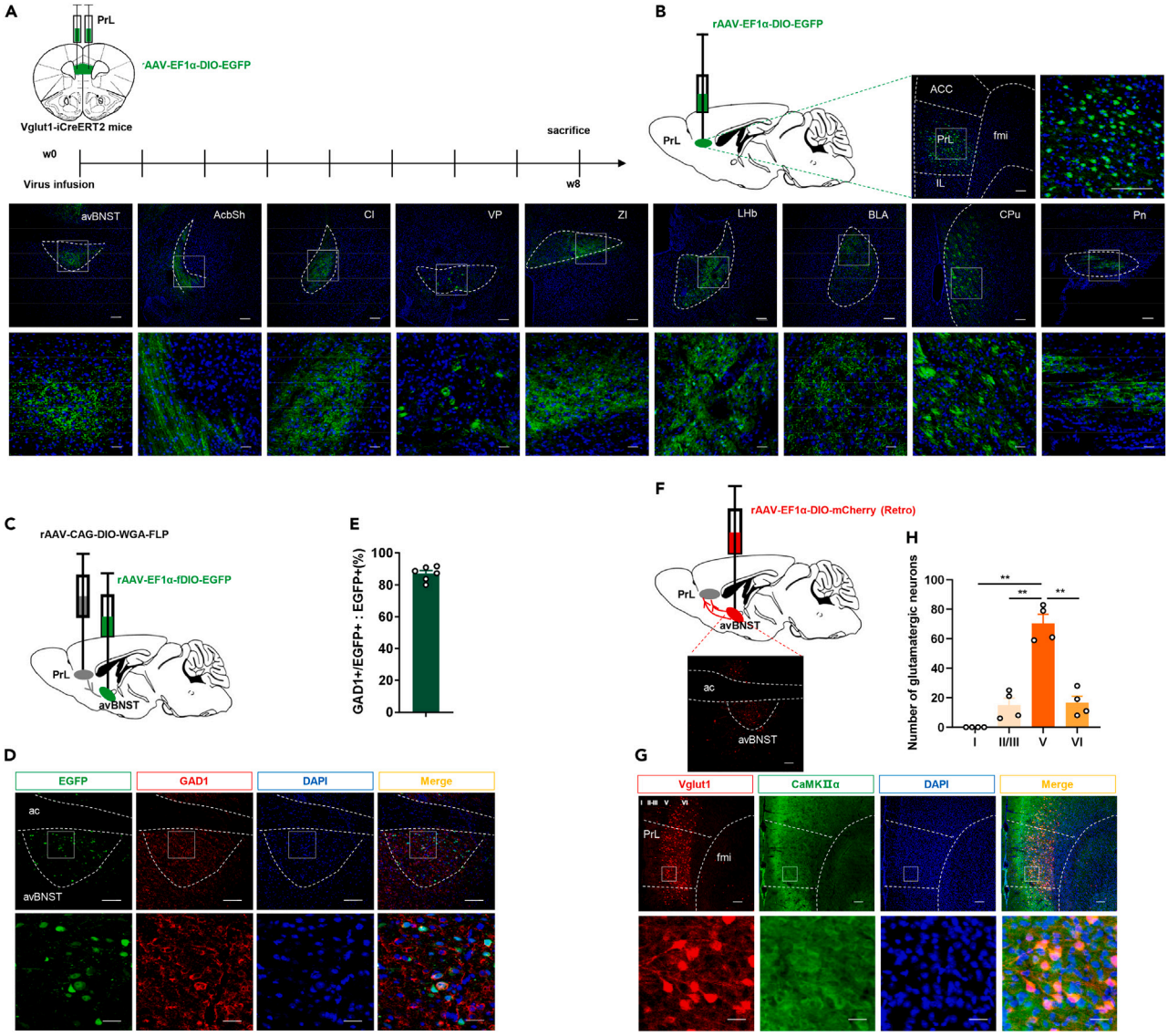

Figure 4. PrL glutamatergic neurons project to the avBNST

(A) Time course of the experiment. The PrL of VGlut1-iCreERT2 mice was injected with rAAV-DIO-EGFP.

(B) Glutamatergic neurons in the PrL project to several brain regions. Cpu, caudate putamen; AcbSh, shell of the nucleus accumbens; Cl, claustrum; VP, ventral pallidum; ZI, zona incerta; LHb, lateral habenular nucleus; BLA, basolateral amygdaloid nucleus; PAG, periaqueductal gray; Pn, pontine nuclei. First and second rows, scale bars = 100 μm. Third row, scale bars = 25 μm.

(C) In VGlut1-iCreERT2 mice, the PrL was injected with rAAV-CAG-DIO-WGA-FLP and the avBNST was injected with rAAV-EF1α-fDIO-EGFP.

(D) Transsynaptic transmission from glutamatergic neurons of PrL to avBNST. Upper panels, scale bar = 100 μm. Lower panels, scale bar = 25 μm.

(E) Co-expression of labeled GABAergic neurons and anti-GAD1 protein was 87.03%.

(F) The avBNST in VGlut1-iCreERT2 mice was injected with rAAV-EF1α-DIO-mCherry (retro).

(G) *In situ* fluorescence imaging of mCherry in the avBNST and fluorescence images for VGlut1 and CaMKIIα protein. Upper panels, scale bar = 100 μm. Lower panels, scale bar = 25 μm.

(H) The number of glutamatergic neurons in layers I–VI (n = 4 mice per group, $^{**}p < 0.01$, one-way ANOVA and Bonferroni post hoc tests). Data are represented as mean ± SEM.

The PrL^{Glu}→avBNST^{GABA} circuit mediates depression-like behaviors

To determine whether the PrL^{Glu}→avBNST^{GABA} circuit mediates depression-like behaviors, we used optogenetics to activate and inhibit PrL^{Glu} terminals in the avBNST. First, we injected rAAV-Ef1α-DIO-eNpHR3.0-mCherry-WPRE-pA or rAAV-Ef1α-DIO-mCherry-WPRE-pA into bilateral PrL in naive VGlut1-iCreERT2 mice and implanted optical fibers above the avBNST. Behavioral tests were conducted 3 weeks

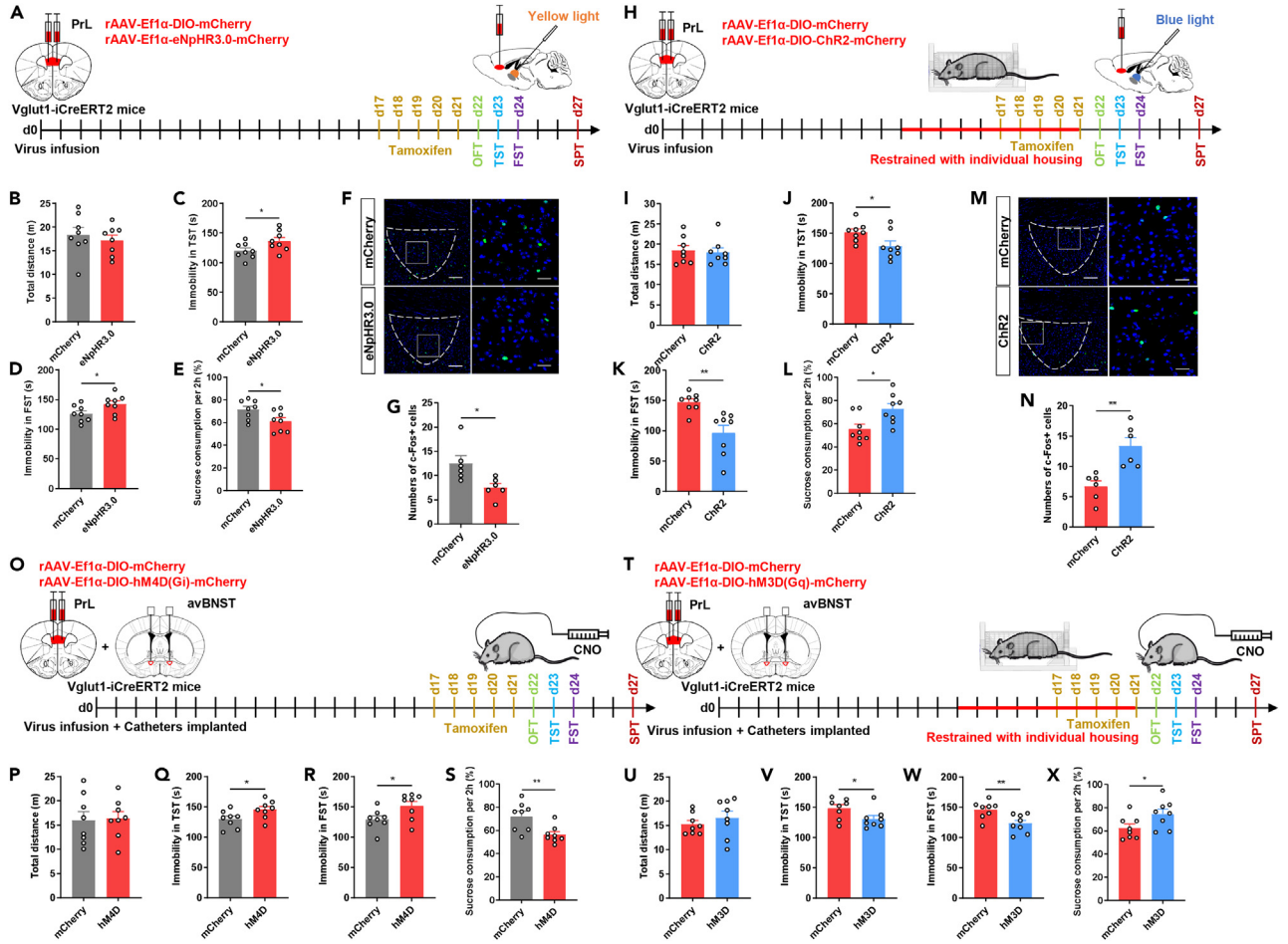

Figure 5. The PrL glutamatergic projection to the avBNST is involved in depression-like behaviors

(A) Time course of the optogenetic-inhibition experiment.

(B–E) Comparison of behavior in the open-field test, tail-suspension test, forced-swim test, and sucrose-preference test in the eNpHR3.0 and mCherry (control) groups (n = 8 mice per group, *p < 0.05, **p < 0.01, two-tailed student's t-tests).

(F) c-Fos expression in the avBNST in the eNpHR3.0 group and the mCherry group. Upper scale bar = 100 μm. Lower scale bar = 25 μm.

(G) Comparison of the number of c-Fos+/DAPI+ cells in the eNpHR3.0 and mCherry groups (n = 6 mice per group, *p < 0.05, two-tailed student's t-tests).

(H) Time course of the optogenetic-activation experiment.

(I–L) Comparison of behavior in the open-field test, tail-suspension test, forced-swim test, and sucrose-preference test between in the ChR2 and mCherry (control) groups (n = 8 mice per group, *p < 0.05, **p < 0.01, two-tailed student's t-tests).

(M) c-Fos expression in the avBNST in the ChR2 group and the mCherry group. Upper scale bar = 100 μm. Lower scale bar = 25 μm.

(N) Comparison of the number of c-Fos+/DAPI+ cells in the ChR2 and mCherry groups (n = 6 mice per group, **p < 0.01, two-tailed student's t-tests).

(O) Time course of the chemogenetic inhibition experiment.

(P–S) Comparison of behavior in the open-field test, tail-suspension test, forcedswim test, and sucrose-preference test in the hM4D and mCherry (control) groups (n = 8 mice per group, *p < 0.05, **p < 0.01, two-tailed student's t-tests).

(T) Time course of the chemogenetic activation experiment.

(U–X) Comparison of behavior in the open-field test, tail-suspension test, forced-swim test, and sucrose-preference test in the hM3D and mCherry groups (n = 8 mice per group, *p < 0.05, **p < 0.01, two-tailed student's t-tests). Data are represented as mean ± SEM.

later under continuous yellow light stimulation (4mW, 589 nm, 9999ms, 0.0001Hz) (Figure 5A). There was no discernible difference in the total distance traveled between the eNpHR3.0 and viral control groups in the open-field test (t_{14} = 0.6202, p > 0.05, Figure 5B), excluding the possibility that changes in the subsequent tests were secondary to locomotor effects. During the tail-suspension test and the forced-swim test, mice in the eNpHR3.0 group time spent more time immobile than mice in the control group (t_{14} = 2.179, p < 0.05, Figure 5C; t_{14} = 2.148, p < 0.05; Figure 5D). Consistent with this, the consumption of sugar water was lower in the eNpHR3.0 group than in the mCherry control group (t_{14} = 2.358, p < 0.05, Figure 5E). Thus, optogenetic inhibition of avBNST-projecting PrL^{Glu} neurons induced depression-like behaviors in naive mice. Yellow light stimulation also reduced the number of c-Fos-positive cells in the avBNST compared with the mCherry group (t_{14} = 2.752,

$p < 0.05$, Figures 5F and 5G). Since the majority of avBNST neurons are GABAergic, this suggests that the optogenetic inhibition of avBNST-projecting glutamatergic neurons in the PrL suppresses GABAergic activity in the avBNST.

Next, we injected rAAV-Ef1α-DIO-ChR2-mCherry-WPRE-pA or rAAV-Ef1α-DIO-mCherry-WPRE-pA into bilateral PrL of VGlut1-iCreERT2 mice, and again implanted optical fibers above the avBNST. Upon the completion of the 10-day chronic restraint stress with individual housing paradigm, the $PrL^{Glu} \rightarrow avBNST^{GABA}$ glutamatergic terminals were photostimulated with blue light (4mW, 473 nm, 5ms, 10 Hz) and depression-like behaviors were evaluated (Figure 5H). As with optogenetic inhibition, no differences were observed in the open-field test ($t_{14} = 0.2872$, $p > 0.05$, Figure 5I). In the tail-suspension test and forced-swim test, the ChR2 group spent less time immobile ($t_{14} = 2.345$, $p < 0.05$, Figure 5J; $t_{14} = 3.689$, $p < 0.01$; Figure 5K) and consumed more sugar water than the mCherry group ($t_{14} = 2.752$, $p < 0.05$, Figure 5L). These results suggest that the optogenetic activation of avBNST-projecting glutamatergic neurons in the PrL triggers an immediate antidepressant effect. We also observed increased expression of c-Fos-positive cells in the ChR2 group compared with the mCherry group ($t_{14} = 3.968$, $p < 0.01$, Figures 5M and 5N), suggesting that the optogenetic activation of avBNST-projecting PrL^{Glu} neurons enhanced the activity of GABAergic neurons in the avBNST.

A similar experiment was performed with the chemogenetic approach. Bilateral drug-delivery catheters were implanted into the avBNST and rAAV-Ef1α-DIO-hM4D(Gi)-mCherry-WPRE-pA, rAAV-Ef1α-DIO-hM3D(Gq)-mCherry-WPRE-pA, or control virus was injected into bilateral PrL in VGlut1-iCreERT2 mice; 3 weeks later, CNO was microinjected through the catheters and behavioral tests were conducted. Consistent with the optogenetic results, the chemogenetic inhibition of PrL^{Glu} terminals in the avBNST induced depression-like behaviors in naive mice (hM4D(Gi): $t_{14} = 0.1555$, $p > 0.05$; $t_{14} = 2.201$, $p < 0.05$; $t_{14} = 2.329$, $p < 0.05$; $t_{14} = 3.143$, $p < 0.01$; Figures 5O–5S) whereas chemogenetic activation led to the amelioration of depression-like behaviors in restraint-stress mice (hM3D(Gq): $t_{14} = 0.8288$, $p > 0.05$; $t_{14} = 2.149$, $p < 0.05$; $t_{14} = 3.095$, $p < 0.01$; $t_{14} = 2.206$, $p < 0.05$; Figures 5T–5X). In sum, these results demonstrate that the $PrL^{Glu} \rightarrow avBNST^{GABA}$ circuit mediates depression-like behavior in mice.

Optogenetic activation of the $PrL^{Glu} \rightarrow avBNST^{GABA}$ circuit ameliorates depression-like behaviors via α-amino-3-hydroxy-5-methyl-4-isoxazole-propionicacid receptors

Ionotropic glutamate receptors, including AMPA receptors (AMPARs) and NMDA receptors (NMDARs), are responsible for rapid excitatory synaptic transmission in the central nervous system. In an attempt to identify the receptor type through which the effects described above are exerted, we combined pharmacological and optogenetic approaches. As shown in Figure 6A, we injected rAAV-Ef1α-DIO-ChR2-mCherry-WPRE-pA into unilateral PrL, implanted an optical fiber into the avBNST, and implanted a catheter into avBNST. Behavioral tests were conducted with simultaneous photostimulation after chronic restraint stress with individual housing. Thirty minutes prior to photostimulation, 150 nL of saline, the NMDAR antagonist MK-801 (1 mM), or the AMPAR antagonist NBQX (1 mM) was administered via the catheter. However, behavioral tests did not reveal any observable differences between the three groups ($F_{2,21} = 0.1734$, $p > 0.05$, Figure 6B; $F_{2,21} = 0.995$, $p > 0.05$; Figure 6C; $F_{2,21} = 0.0095$, $p > 0.05$; Figure 6D; $F_{2,21} = 1.023$, $p > 0.05$; Figure 6E). The concentration of antagonist was therefore increased to 10 mM. Mice in all groups traveled a similar distance in the open-field test ($F_{2,21} = 0.1279$, $p > 0.05$, Figure 6F). The 10 mM NBQX group spent more time immobile in the tail-suspension test ($F_{2,21} = 3.782$, $p < 0.05$, Figure 6G) and forced-swim test ($F_{2,21} = 5.778$, $p < 0.05$, Figure 6H) and had lower sugar-water consumption ($F_{2,21} = 5.322$, $p < 0.05$, Figure 6I) than the saline group, but the MK-801 group did not. In other words, NBQX but not MK-801 blocked the effects of optogenetic activation. In addition, pharmacological inhibition of AMPARs but not NMDARs in avBNST induced depression-like behaviors in mice (Figure S2). The above suggesting that the antidepressant effect of circuit activation may be mediated via AMPARs rather than NMDARs.

The $PrL^{Glu} \rightarrow avBNST^{GABA}$ circuit contributes to the rapid-acting antidepressant effect of ketamine

Ketamine is a rapid-acting antidepressant used in research on depression. To determine the effect of ketamine on avBNST-projecting PrL glutamatergic neurons, we performed fiber photometry recordings during the tail-suspension test in restraint-stressed mice that had received a dose of either ketamine or saline. rAAV-CaMKIIα-Cre-WPRE-PA (retro) virus was injected into the avBNST of C57BL/6J mice and rAAV-Ef1α--DIO-GCaMp6s-WPRE-PA was injected into the PrL. An optical fiber was embedded in the PrL and fixed in place with dental cement (Figure 7A). Three weeks later, we evaluated Ca^{2+} transients before (baseline) (Figure 7D) and after (Figure 7E) 10 days of chronic restraint stress with individual housing (restraint), and again 24 h after ketamine (10 mg/kg, ip) administration (restraint+ketamine) (Figure 7F). Because the genetically encoded calcium sensor (GCaMP6s) was reliably expressed, we could measure activity repeatedly from the same population of cells. We analyzed Ca^{2+} transients synchronized with struggling (motivated avoidance behavior) in the tail-suspension test. Struggling behaviors were associated with a burst in Ca^{2+} transients. We calculated the area under the Ca^{2+} signaling curve to assess neuronal activity. The AUC was reduced after chronic restraint stress with individual housing, but returned to baseline after ketamine administration ($F_{1.915,\ 9.577} = 18.2$, $p < 0.01$, Figure 7B). This indicates that ketamine rapidly rescued the dysfunction in the $PrL^{Glu} \rightarrow avBNST^{GABA}$ circuit the resulted from chronic restraint stress with individual housing.

To probe this further, we combined optogenetic and pharmacological approaches with behavioral tests and ketamine administration in VGlut1-iCreERT2 mice that had undergone chronic restraint stress with individual housing (Figure 7G). Mice were randomly divided into four groups: an mCherry+saline group, an mCherry+ketamine group, an eNpHR3.0+saline group, and an eNpHR3.0+ketamine group. We used the same ketamine administration regimen as described above. Photoinhibition of terminals was delivered via an optical fiber in the avBNST and behavioral test were conducted 1 h after saline or ketamine administration. In the open-field test, no significant variation in motor ability was observed among the four groups ($F_{3,28} = 0.6339$, $p > 0.05$, Figure 7H). Mice in the mCherry+ketamine group spent less time immobile in

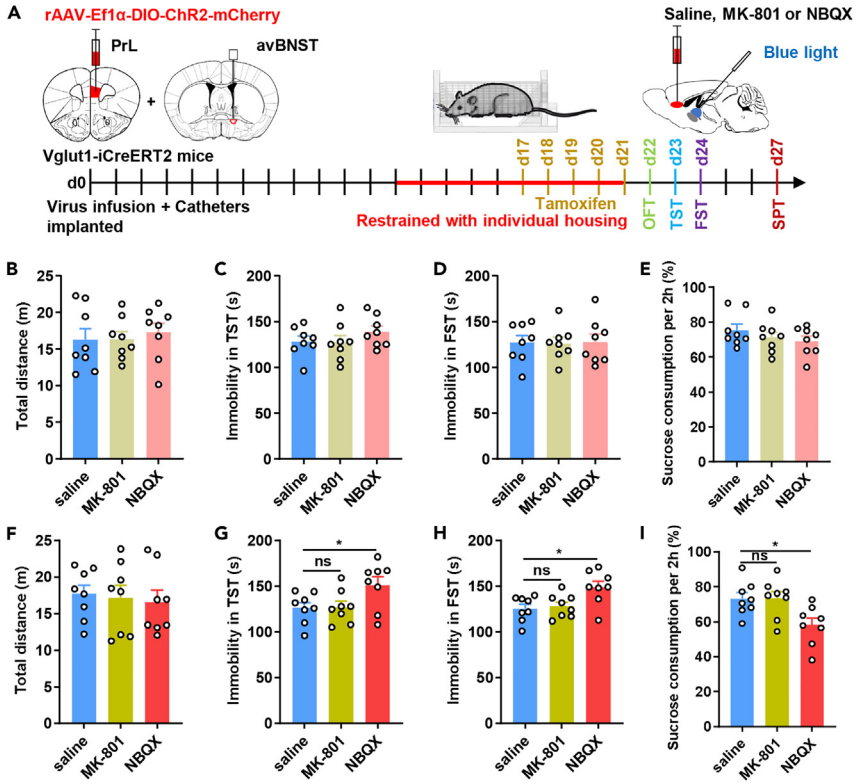

Figure 6. Optogenetic activation of the PrL^{Glu}→avBNST^{GABA} projection alleviates depression-like behaviors via AMPARs but not NMDARs

(A) Timeline of the virus injections, induction of stress, drug administration, and behavioral tests.

(B–E) Comparison of behavior in the open-field test, tail-suspension test, forced-swim test, and sucrose-preference test in the saline, MK-801 (1 mM), and NBQX (1 mM) groups.

(F–I) Comparison of behavior in the open-field test, tail-suspension test, forced-swim test, and sucrose-preference test in the saline, MK-801 (10 mM) and NBQX (10 mM) groups (n = 8 mice per group, *p < 0.05, one-way ANOVA and Bonferroni post hoc tests). Data are represented as mean ± SEM.

the tail-suspension and forced-swim tests than mice in the mCherry+saline group ($F_{3,28}$ = 25.2, p < 0.01, Figure 7I; $F_{3,28}$ = 23.24, p < 0.01; Figure 7J) and had increased consumption of sugar water ($F_{3,28}$ = 13.95, p < 0.01, Figure 7K), providing evidence that ketamine produced a potent antidepressant effect. Optogenetic inhibition of PrL^{Glu} terminals in the avBNST diminished the rapid antidepressant effect seen in the eNpHR3.0+ketamine group compared with the mCherry+ketamine group. However, when we compared the eNpHR3.0+saline group with the eNpHR3.0+ketamine group, we observed that the yellow light stimulation did not completely ablate the rapid antidepressant effect of ketamine (Figures 7I–7K).

In summary, the decreased activity of avBNST-projecting glutamatergic PrL neurons due to chronic restraint stress with individual housing could be quickly restored by ketamine, and the PrL^{Glu}→avBNST^{GABA} circuit in part mediated this rapid antidepressant effect of ketamine. These results suggest that the PrL^{Glu}→avBNST^{GABA} circuit is not only involved in depression-like behaviors, but also mediates the depression-like behaviors rapidly.

Ketamine rapidly rescues the restraint-stress-induced decrease in the activity of anterior ventral bed nucleus of the stria terminalis GABAergic neurons

We have already demonstrated the projection from glutamatergic neurons of the PrL to GABAergic neurons of avBNST, as well as the influence of glutamatergic activity on GABAergic activity. In order to determine the role of avBNST GABAergic neurons in depression-like behaviors, we used fiber photometry to measure the Ca^{2+} fluorescence signals from these neurons during the tail-suspension test. We recorded the Ca^{2+} signal before (baseline) and after (restraint) chronic restraint stress with individual housing, and again 24 h after ketamine treatment (restraint+ketamine), as described above. To record specifically from GABAergic neurons, we used Vgat-Cre mice. rAAV-Ef1α-DIO-GCaMp6s-WPRE-pA was microinjected into the avBNST of Vgat-Cre mice (Figure 8A). The increase in fluorescence intensity of GCaMP6s correlated well with the onset of struggle events in mice (Figures 8D–8F). We observed that the AUC decreased after chronic restraint stress with individual housing, but this effect was reversed by ketamine ($F_{1.245,\ 6.223}$ = 19.92, p < 0.01, Figure 8B). This suggests that ketamine rapidly mitigated the changes in activity in avBNST GABAergic neurons caused by chronic restraint stress with individual housing.

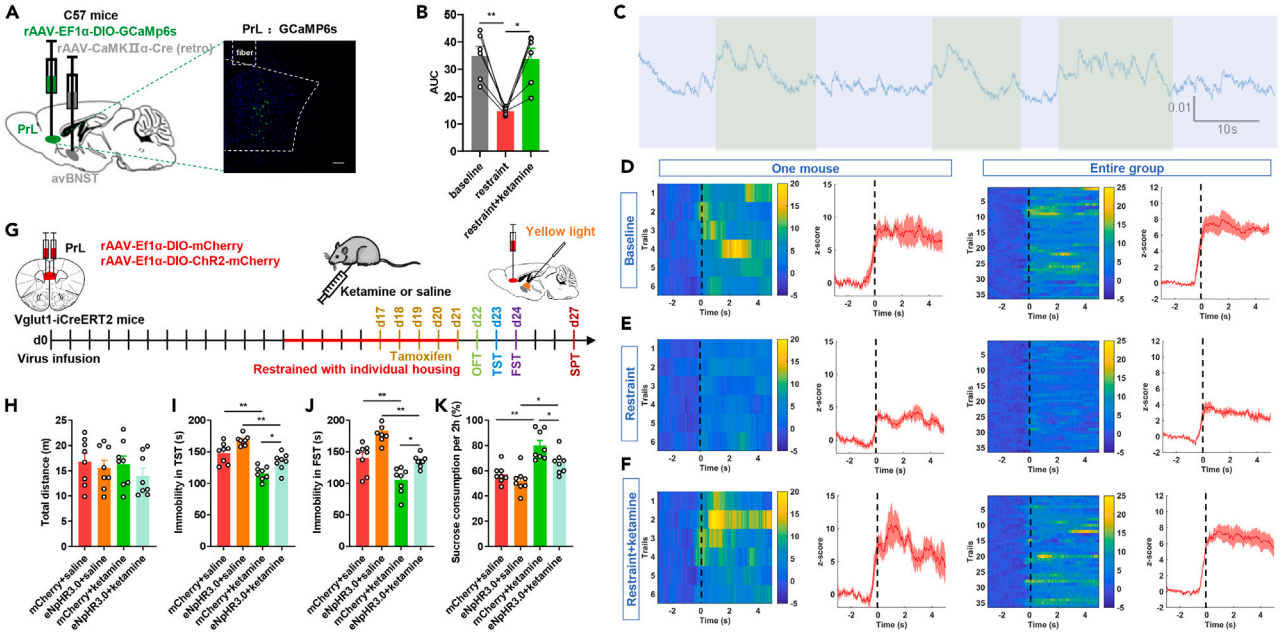

Figure 7. The PrL^{Glu}→avBNST^{GABA} circuit plays a role in to the rapid antidepressant effect of ketamine

(A) Fluorescence image of GCaMP6s expressed in the PrL. Scale bar = 100 μm.

(B) Summary of struggle-locked AUC data (n = 6 mice per group, *p < 0.05, **p < 0.01, mixed-effects ANOVA and Bonferroni post hoc tests).

(C) Example fluorescence trace from avBNST GABAergic neurons during the tail-suspension test. Green regions indicate struggle events.

(D) Left panels, heat maps and summary plot for Ca^{2+} signals time-locked to the initiation of individual struggle events in a single baseline mouse. In the heatmap, each event is plotted in one row. In the summary plot, solid lines indicate the mean and the shaded areas represent the SEM. Right panels, same as left panels but for all mice (n = 6 mice per group).

(E) Same as panel d but for the restraint group.

(F) Same as panel d but for the restraint+ketamine group.

(G) Timeline of virus injection, model establishment, drug administration, and behavioral tests for the optogenetic inhibition experiment.

(H–K) Comparison of behavior in the open-field test, tail-suspension test, forced-swim test and sucrose-preference test in the mCherry+saline, mCherry+ketamine, eNpHR3.0+saline, and eNpHR3.0+ketamine groups (n = 8 mice per group, *p < 0.05, **p < 0.01, one-way ANOVA and Bonferroni post hoc tests). Data are represented as mean ± SEM.

DISCUSSION

The burden of depression on society hinders society's development and stability.[31] Examining the neural circuit mechanisms of depression and paying attention to the mechanisms and efficacy of rapid-acting antidepressants is essential if we are to improve the treatment of clinical depression.

One of the benefits of investigating the neural circuit of a disease is the ability to pinpoint the convergence of regions involved in pathological behavior and response to medication. Consistent with this notion, we successfully established a depression model that combined chronic restraint stress and individual housing. First, we found that glutamatergic neurons in the PrL mediate depression-like behaviors and are transsynaptically connected to GABAergic neurons in avBNST. Second, we found that the activation of the PrL^{Glu}→avBNST^{GABA} circuit mediates antidepression-like effects via AMPARs but not NMDARs. Third, we found that ketamine normalizes the chronic-stress-induced dysregulation of the PrL^{Glu}→avBNST^{GABA} projection. Consistent with this, the rapid-acting antidepressant effect of ketamine was weakened by the optogenetic inhibition of PrL^{Glu}→avBNST^{GABA} axons. These results indicate that the PrL^{Glu}→avBNST^{GABA} projection can rapidly regulate depression-like behaviors and that the fast antidepressant effect of ketamine is partly mediated through this circuit.

Only male mice were used in this experiment. This is because we found that female mice did not show depression-like behaviors after experiencing chronic restraint stress with individual housing. One reason for this is that estrogen and progesterone disturbances during the estrous cycle may affect behavioral tests and potentially depression-related circuits, but it has also been shown that testosterone levels similarly affect outcomes.[32,33] What's more, studies have shown that male and female mice have different brain regions and mechanisms associated with depression-like behaviors[34,35] and respond differently to different stresses, as suggested by Iqbal et al. that subchronic variable stress (SCVS) induced depression-like behaviors in female rats only and the chronic unpredictable mild stress (CUMS) was more likely to induce depression-like behaviors in male rats.[36] The ideal model of depression in female mice may require further research and development.

We selected this brain region for our study because the mPFC is a key brain region associated with depression. Of the three subregions of the mPFC, the ACC and the PrL are associated with the regulation of emotion, but the ACC is mainly involved in pain-related affective disorders.[37] Studies have shown that decreased density of the perineuronal net in the PrL is linked to depression-like behaviors[38]; furthermore,

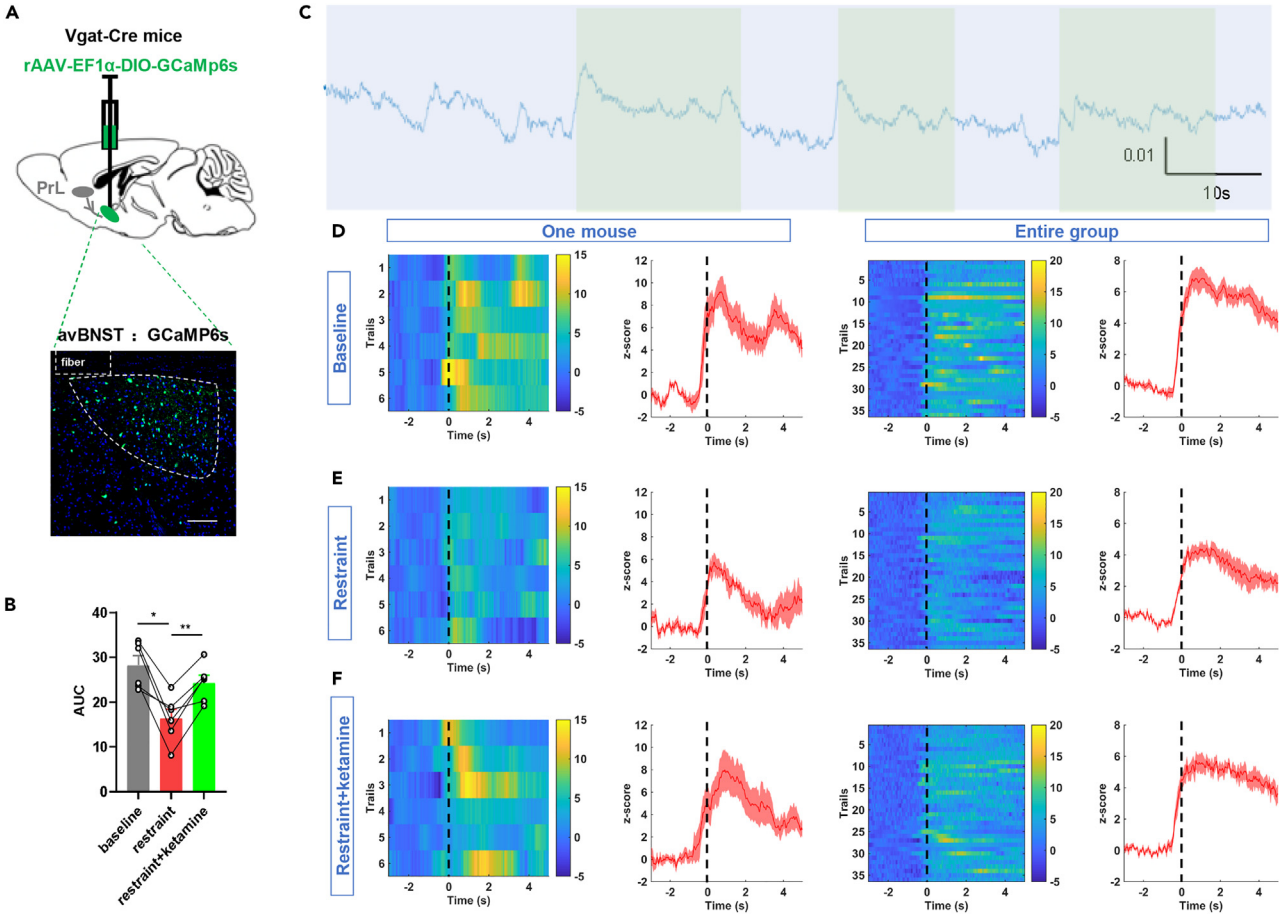

Figure 8. Ketamine rapidly rescues the decrease in avBNST GABAergic activity induced by chronic restraint stress with individual housing

(A) Fluorescence image of GCaMP6s expressed in the avBNST of Vgat-Cre mice. Scale bar = 100 μm.

(B) Summary of struggle-locked AUC data (n = 6 mice per group, *p < 0.05, **p < 0.01, mixed-effects ANOVA and Bonferroni post hoc tests).

(C) Example fluorescence trace from avBNST GABAergic neurons during the tail-suspension test. Green indicates struggle events.

(D) Left panels, heat maps and summary plot for Ca^{2+} signals time-locked to the initiation of individual struggle events in a single baseline mouse. In the heatmap, each event is plotted in one row. In the summary plot, solid lines indicate the mean and the shaded areas represent the SEM. Right panels, same as left panels but for all mice (n = 6 mice per group).

(E) Same as panel d but for the restraint group.

(F) Same as panel d but for the restraint+ketamine group. Data are represented as mean ± SEM.

chronic variable stress alters the dendritic spine subtypes in the PrL decreases levels of Fos expression.[39] Consistent with this, we found that chronic restraint stress with individual housing led to decreased activity of glutamatergic neurons in the PrL. A two-photon calcium-imaging study in the mPFC showed that, with chronic CORT treatment, the proportion of simultaneously active cells is reduced and the frequency of multicellular ensemble events decreases.[40] Here, our study further clarified the critical role of glutamatergic neurons in the PrL subregion using VGlut1-iCreERT2 mice and viral techniques.

The BNST is downstream of the PrL, and numerous studies have demonstrated its role in integrating information to modulate stress, anxiety, and depression.[41] In patients with major depressive disorder, BNST deep-brain stimulation achieved sustained remission of depression.[42] The BNST is believed to affect depression-like behaviors through cell-type-specific excitatory/inhibitory synaptic balance.[43] This balance is influenced by inputs from other brain regions. I also mentioned that in the introduction that hyperactivity of the HPA axis is one of the important pathogenic mechanisms of depression. GABAergic neurons in avBNST play a vital role in suppressing the HPA axis in stress.[21,44] Activation of the HPA axis is regulated by a network of interconnected cell populations in the limbic forebrain. However, these limbic forebrain regions do not directly innervate HPA effector cell populations in the paraventricular hypothalamus (PVH).[45] Studies show that avBNST acts as a point of convergence between the limbic forebrain and PVH. Anatomical tracing experiments confirmed projections from PrL to implicated aBNST cell groups, and from these to PVH.[15] Because of these previous studies, we hypothesized that the $PrL^{Glu} \rightarrow avBNST\text{-}^{GABA}$ projection may play a role in depression. We confirmed that the activation of AV-projecting PrL glutamatergic neurons by either

optogenetic or chemogenetic manipulations ameliorates depression-like behaviors induced in mice by chronic restraint stress combined with individual housing.

Depression is considered a multi-regional network-regulation disorder. In fMRI studies of the pathophysiology of depression, large-scale brain networks show prominent abnormalities in participants with depression, most notably localized neuronal inefficiency in mPFC along with wider network-level disruptions.[46] This suggests that depression involves interactions between multiple brain regions and circuits, rather than a single circuit. This could also explain why the PrL projection examined here was only partly responsible for the rapid antidepressant effect of ketamine: other circuits—such as mPFC→VTA and mPFC→BLA—may also be involved.[47] Several other circuits positively or negatively regulate depression-like behaviors, for instance entorhinal cortex → medial secondary visual cortex (Ent → V2M),[48] mPFC→ dorsal raphe nucleus (DRN),[49] lateral habenula → rostromedial tegmental nucleus (LHb→RMTg),[50] and mPFC→NAc.[51] In particular, the activation of glutamatergic mPFC neurons that project to the DRN produces an antidepressant effect in mice, and optogenetic activation of mPFC axon terminals in the NAc promotes depressive responses. Different multi-regional brain networks appear to exert positive and negative effects on emotions and the behavioral phenotypes associated with them. Maintaining a stable psychological state relies on the coordination of both kinds of networks. Our experiment further clarified our knowledge of these multi-regional networks: activation of the PrL→avBNST circuit has an antidepressant effect so this circuit forms part of the positive network.

Prior research into the circuit mechanims of depression has been restricted to overall effects on depression. In this study, we specifically examined the speed of the antidepressant effect. We used ketamine validation experiments to demonstrate that the PrL^{Glu}→$avBNST^{GABA}$ modulation of depression occurs rapidly and to begin to probe the molecular mechanisms that underlie the speed of the effect. Ketamine dramatically increases the activity of pyramidal neurons in the mPFC and exerts an antidepressant-like action, but fluoxetine had no such effects under the same conditions.[52] Although both drugs are antidepressants, fluoxetine has a much slower onset of action.[53] This suggests that the mPFC may be a good target region for rapid-acting antidepressant treatments. One point of interest is the apparent increase of neuronal activity prior to the onset of the struggle behavior. This may reflect the fact that PrL glutamate neurons drove the initiation struggle behavior, which showed the distinct temporal dynamics. It has been shown that the mPFC is critical for decisions related to reward and aversion learning, which are the ultimate drivers of behavior.[54] Here, struggling in mice can also be considered an aversive behavior, and thus neuronal activity in PrL drives struggling behavior. Studies also found that prefrontal striatal circuits are critical for temporal control of actions,[55] and thus top-down control of avBNST by PrL may also be involved. Ionotropic and metabotropic glutamate receptors are the major classes of glutamate receptors, with ionotropic receptors mediating fast signaling and metabotropic receptors regulating slower responses.[56] Ionotropic receptors include NMDARs and AMPARs. Because the single-channel conductance of AMPARs is lower than NMDARs, excitatory synaptic transmission via AMPARs is faster than transmission via NMDARs.[57] AMPAR agonists and positive allosteric modulators can be effective as rapid-acting antidepressants.[58] In addition, the fast antidepressant effect of ketamine can be offset by AMPAR antagonists.[59] We found that antagonizing AMPARs, but not NMDARs, prevented the rapid alleviation of depression-like behaviors, suggesting not only that AMPARs contribute significantly to the circuit but also that the PrL^{Glu}→$avBNST^{GABA}$ projection modulates depression-like behaviors in a rapid fashion.

The translational implications of a study are a reliable indicator of its impact. The current study has the potential to translate into clinical treatment for depression. Nonpharmacological therapies—e.g., electroshock and transcranial magnetic stimulation[60,61] —can cause side effects such as nausea and vomiting, amnesia, and cognitive dysfunction due to the extensive stimulation of the brain[62]; our study potentially allows for precise targeting to reduce unnecessary functional impairments. Furthermore, clarifying the connectivity patterns and specific functions of circuits facilitates non-pharmaceutical therapies such as emotion-based brain–computer interfaces (BCIs)[63] by complementing the datasets used by the BCIs.

In summary, our study demonstrates that, in mice, the PrL^{Glu}→$avBNST^{GABA}$ projection mediates rapid modulation of depression-like behaviors induced by chronic restraint stress combined with individual housing. Our results support the idea of circuit-based treatments for depression, provide a perspective on advancing past traditional monoamine-based treatment strategies, and suggest a promising new avenue of investigation for the development of fast antidepressants.

Limitations of the study

We used regular bottles for sucrose-preference test. A specialized device has been demonstrated to improve the accuracy of sucrose-preference test and could be considered for use in the future.

The machines for fiber photometry are monochrome channel, and machines with two or even three color channels have been developed to improve the sensitivity and accuracy of fiber photometry measurements, and these more advanced machines can be considered in the future.

STAR★METHODS

Detailed methods are provided in the online version of this paper and include the following:

- KEY RESOURCES TABLE
- RESOURCE AVAILABILITY
  - Lead contact
  - Materials availability
  - Data and code availability
- EXPERIMENTAL MODEL AND STUDY PARTICIPANT DETAILS

SUPPLEMENTAL INFORMATION

Supplemental information can be found online at https://doi.org/10.1016/j.isci.2023.107878.

ACKNOWLEDGMENTS

The present study was supported by the National Key R&D Program of China (2021ZD0203100), the National Natural Science Foundation of China (Grant Numbers 82271257, 82071228).

AUTHOR CONTRIBUTIONS

CJY: Writing - original draft, Investigation, Formal analysis, Data curation; WK: Investigation; GMM: Data curation; SW: Validation; HST: Validation; ZYM: Conceptualization, Writing - review & editing, Funding acquisition.

DECLARATION OF INTERESTS

The authors declare that they have no conflict of interest.

INCLUSION AND DIVERSITY

We support inclusive, diverse, and equitable conduct of research.

Received: February 9, 2023
Revised: June 20, 2023
Accepted: September 7, 2023
Published: September 12, 2023

REFERENCES

1. Herrman, H., Patel, V., Kieling, C., Berk, M., Buchweitz, C., Cuijpers, P., Furukawa, T.A., Kessler, R.C., Kohrt, B.A., Maj, M., et al. (2022). Time for united action on depression: a Lancet-World Psychiatric Association Commission. Lancet *399*, 957–1022. https://doi.org/10.1016/S0140-6736(21)02141-3.
2. Simon, G.E., Shortreed, S.M., Rossom, R.C., Beck, A., Clarke, G.N., Whiteside, U., Richards, J.E., Penfold, R.B., Boggs, J.M., and Smith, J. (2022). Effect of Offering Care Management or Online Dialectical Behavior Therapy Skills Training vs Usual Care on Self-harm Among Adult Outpatients With Suicidal Ideation: A Randomized Clinical Trial. JAMA *327*, 630–638. https://doi.org/10.1001/jama.2022.0423.
3. Lewis, G., Marston, L., Lewis, G., ANTLER study team, Gilbody, S., Hunter, R., Kendrick, T., Kessler, D., Mangin, D., King, M., et al. (2021). Maintenance or Discontinuation of Antidepressants in Primary Care. N. Engl. J. Med. *385*, 2587–2588. https://doi.org/10.1056/NEJMc2117168.
4. Coleman, J.A., Yang, D., Zhao, Z., Wen, P.C., Yoshioka, C., Tajkhorshid, E., and Gouaux, E. (2019). Serotonin transporter-ibogaine complexes illuminate mechanisms of inhibition and transport. Nature *569*, 141–145. https://doi.org/10.1038/s41586-019-1135-1.
5. Szuhany, K.L., and Otto, M.W. (2020). Assessing BDNF as a mediator of the effects of exercise on depression. J. Psychiatr. Res. *123*, 114–118. https://doi.org/10.1016/j.jpsychires.2020.02.003.
6. Daws, R.E., Timmermann, C., Giribaldi, B., Sexton, J.D., Wall, M.B., Erritzoe, D., Roseman, L., Nutt, D., and Carhart-Harris, R. (2022). Increased global integration in the brain after psilocybin therapy for depression. Nat. Med. *28*, 844–851. https://doi.org/10.1038/s41591-022-01744-z.
7. Porter, J.T., and Sepulveda-Orengo, M.T. (2020). Learning-induced intrinsic and synaptic plasticity in the rodent medial prefrontal cortex. Neurobiol. Learn. Mem. *169*, 107117. https://doi.org/10.1016/j.nlm.2019.107117.
8. Klune, C.B., Jin, B., and DeNardo, L.A. (2021). Linking mPFC circuit maturation to the developmental regulation of emotional memory and cognitive flexibility. Elife *10*, e64567. https://doi.org/10.7554/eLife.64567.
9. Xu, J., Guo, C., Liu, Y., Wu, G., Ke, D., Wang, Q., Mao, J., Wang, J.Z., Liu, R., and Wang, X. (2020). Nedd4l downregulation of NRG1 in the mPFC induces depression-like behaviour in CSDS mice. Transl. Psychiatry *10*, 249. https://doi.org/10.1038/s41398-020-00935-x.
10. Fisher, B.M., Saksida, L.M., Robbins, T.W., and Bussey, T.J. (2020). Functional dissociations between subregions of the medial prefrontal cortex on the rodent touchscreen continuous performance test (rCPT) of attention. Behav. Neurosci. *134*, 1–14. https://doi.org/10.1037/bne0000338.

11. Shi, X., Zhang, Q., Li, J., Liu, X., Zhang, Y., Huang, M., Fang, W., Xu, J., Yuan, T., Xiao, L., et al. (2021). Disrupting phosphorylation of Tyr-1070 at GluN2B selectively produces resilience to depression-like behaviors. Cell Rep. *36*, 109612. https://doi.org/10.1016/j.celrep.2021.109612.
12. Stubbeman, W.F., Zarrabi, B., Bastea, S., Ragland, V., and Khairkhah, R. (2018). Bilateral neuronavigated 20Hz theta burst TMS for treatment refractory depression: An open label study. Brain Stimul. *11*, 953–955. https://doi.org/10.1016/j.brs.2018.04.012.
13. Blumberger, D.M., Vila-Rodriguez, F., Thorpe, K.E., Feffer, K., Noda, Y., Giacobbe, P., Knyahnytska, Y., Kennedy, S.H., Lam, R.W., Daskalakis, Z.J., and Downar, J. (2018). Effectiveness of theta burst versus high-frequency repetitive transcranial magnetic stimulation in patients with depression (THREE-D): a randomised non-inferiority trial. Lancet *391*, 1683–1692. https://doi.org/10.1016/S0140-6736(18)30295-2.
14. Ährlund-Richter, S., Xuan, Y., van Lunteren, J.A., Kim, H., Ortiz, C., Pollak Dorocic, I., Meletis, K., and Carlén, M. (2019). A whole-brain atlas of monosynaptic input targeting four different cell types in the medial prefrontal cortex of the mouse. Nat. Neurosci. *22*, 657–668. https://doi.org/10.1038/s41593-019-0354-y.
15. Radley, J.J., Gosselink, K.L., and Sawchenko, P.E. (2009). A discrete GABAergic relay mediates medial prefrontal cortical inhibition of the neuroendocrine stress response. J. Neurosci. *29*, 7330–7340. https://doi.org/10.1523/JNEUROSCI.5924-08.2009.
16. Weis, C.N., Huggins, A.A., Bennett, K.P., Parisi, E.A., and Larson, C.L. (2019). High-Resolution Resting-State Functional Connectivity of the Extended Amygdala. Brain Connect. *9*, 627–637. https://doi.org/10.1523/JNEUROSCI.5924-08.2009.
17. Han, Z.S., and Ju, G. (1990). Bed nucleus of the stria terminalis. Sheng Li Ke Xue Jin Zhan *21*, 361–363.
18. Rodríguez-Sierra, O.E., Turesson, H.K., and Pare, D. (2013). Contrasting distribution of physiological cell types in different regions of the bed nucleus of the stria terminalis. J. Neurophysiol. *110*, 2037–2049. https://doi.org/10.1152/jn.00408.2013.
19. Giardino, W.J., Eban-Rothschild, A., Christoffel, D.J., Li, S.B., Malenka, R.C., and de Lecea, L. (2018). Parallel circuits from the bed nuclei of stria terminalis to the lateral hypothalamus drive opposing emotional states. Nat. Neurosci. *21*, 1084–1095. https://doi.org/10.1038/s41593-018-0198-x.
20. Yamauchi, N., Sato, K., Sato, K., Murakawa, S., Hamasaki, Y., Nomura, H., Amano, T., and Minami, M. (2022). Chronic pain-induced neuronal plasticity in the bed nucleus of the stria terminalis causes maladaptive anxiety. Sci. Adv. *8*, eabj5586. https://doi.org/10.1126/sciadv.abj5586.
21. Choi, D.C., Evanson, N.K., Furay, A.R., Ulrich-Lai, Y.M., Ostrander, M.M., and Herman, J.P. (2008). The anteroventral bed nucleus of the stria terminalis differentially regulates hypothalamic-pituitary-adrenocortical axis responses to acute and chronic stress. Endocrinology *149*, 818–826. https://doi.org/10.1210/en.2007-0883.
22. Huang, S.T., Song, Z.J., Liu, Y., Luo, W.C., Yin, Q., and Zhang, Y.M. (2021). BNSTAVGABA-PVNCRF Circuit Regulates Visceral Hypersensitivity Induced by Maternal Separation in Vgat-Cre Mice. Front. Pharmacol. *12*, 615202. https://doi.org/10.3389/fphar.2021.615202.
23. Qin, X.Y., Shan, Q.H., Fang, H., Wang, Y., Chen, P., Xiong, Z.Q., Swaab, D.F., and Zhou, J.N. (2021). PSD-93 up-regulates the synaptic activity of corticotropin-releasing hormone neurons in the paraventr icular nucleus in depression. Acta Neuropathol. *142*, 1045–1064. https://doi.org/10.1007/s00401-021-02371-7.
24. Lambert, P.M., Lu, X., Zorumski, C.F., and Mennerick, S. (2022). Physiological markers of rapid antidepressant effects of allopregnanolone. J. Neuroendocrinol. *34*, e13023. https://doi.org/10.1111/jne.13023.
25. Pehrson, A.L., Roberts, D., Khawaja, A., and McNair, R. (2022). The role of serotonin neurotransmission in rapid antidepressant actions. Psychopharmacology *239*, 1823–1838. https://doi.org/10.1007/s00213-022-06098-5.
26. Zhang, H., Sun, Y., Yau, S.Y., Zhou, Y., Song, X., Zhang, H.T., Zhu, B., Wu, H., and Chen, G. (2022). Synergistic effects of two naturally occurring iridoids in eliciting a rapid antidepressant action by up-regulating hippocampal PACAP signalling. Br. J. Pharmacol. *179*, 4078–4091. https://doi.org/10.1111/bph.15847.
27. Berman, R.M., Cappiello, A., Anand, A., Oren, D.A., Heninger, G.R., Charney, D.S., and Krystal, J.H. (2000). Antidepressant effects of ketamine in depressed patients. Biol. Psychiatr. *47*, 351–354. https://doi.org/10.1016/s0006-3223(99)00230-9.
28. Shiroma, P.R., Thuras, P., Wels, J., Albott, C.S., Erbes, C., Tye, S., and Lim, K.O. (2020). A randomized, double-blind, active placebo-controlled study of efficacy, safety, and durability of re peated vs single subanesthetic ketamine for treatment-resistant depression. Transl. Psychiatry *10*, 206. https://doi.org/10.1038/s41398-020-00897-0.
29. Li, Y., Liu, Z., Guo, Q., and Luo, M. (2019). Long-term Fiber Photometry for Neuroscience Studies. Neurosci. Bull. *35*, 425–433. https://doi.org/10.1007/s12264-019-00379-4.
30. Liu, R.J., Duman, C., Kato, T., Hare, B., Lopresto, D., Bang, E., Burgdorf, J., Moskal, J., Taylor, J., Aghajanian, G., and Duman, R.S. (2017). GLYX-13 Produces Rapid Antidepressant Responses with Key Synaptic and Behavioral Effects Distinct from Ketamine. Neuropsychopharmacology *42*, 1231–1242. https://doi.org/10.1038/npp.2016.202.
31. Herrman, H., Kieling, C., McGorry, P., Horton, R., Sargent, J., and Patel, V. (2019). Reducing the global burden of depression: a Lancet-World Psychiatric Association Commission. Lancet *393*, e42–e43. https://doi.org/10.1016/S0140-6736(18)32408-5.
32. Levy, D.R., Hunter, N., Lin, S., Robinson, E.M., Gillis, W., Conlin, E.B., Anyoha, R., Shansky, R.M., and Datta, S.R. (2023). Mouse spontaneous behavior reflects individual variation rather than estrous state. Curr. Biol. *33*, 1358–1364.e4. https://doi.org/10.1016/j.cub.2023.02.035.
33. Shansky, R.M. (2019). Are hormones a "female problem" for animal research? Science *364*, 825–826. https://doi.org/10.1126/science.aaw7570.
34. Jacobson, L. (2019). Glucocorticoid receptor deletion from locus coeruleus norepinephrine neurons promotes depression-like social withdrawal in female but not male mice. Brain Res. *1710*, 82–91. https://doi.org/10.1016/j.brainres.2018.12.026.
35. Zhang, S., Zhang, H., Ku, S.M., Juarez, B., Morel, C., Tzavaras, N., Montgomery, S., Hodes, G.E., Brancato, A., Russo, S.J., et al. (2018). Sex Differences in the Neuroadaptations of Reward-related Circuits in Response to Subchronic Variable Stress. Neuroscience *376*, 108–116. https://doi.org/10.1016/j.neuroscience.2018.02.021.
36. Iqbal, J., Adu-Nti, F., Wang, X., Qiao, H., and Ma, X.M. (2020). Sex difference in depression: Which animal models mimic it. Behav. Neurosci. *134*, 248–266. https://doi.org/10.1037/bne0000369.
37. Barthas, F., Sellmeijer, J., Hugel, S., Waltisperger, E., Barrot, M., and Yalcin, I. (2015). The anterior cingulate cortex is a critical hub for pain-induced depression. Biol. Psychiatr. *77*, 236–245. https://doi.org/10.1016/j.biopsych.2014.08.004.
38. Yu, Z., Chen, N., Hu, D., Chen, W., Yuan, Y., Meng, S., Zhang, W., Lu, L., Han, Y., and Shi, J. (2020). Decreased Density of Perineuronal Net in Prelimbic Cortex Is Linked to Depressive-Like Behavior in Yo ung-Aged Rats. Front. Mol. Neurosci. *13*, 4. https://doi.org/10.3389/fnmol.2020.00004.
39. Radley, J.J., Anderson, R.M., Hamilton, B.A., Alcock, J.A., and Romig-Martin, S.A. (2013). Chronic stress-induced alterations of dendritic spine subtypes predict functional decrements in an hy pothalamo-pituitary-adrenal-inhibitory prefrontal circuit. J. Neurosci. *33*, 14379–14391. https://doi.org/10.1523/JNEUROSCI.0287-13.2013.
40. Moda-Sava, R.N., Murdock, M.H., Parekh, P.K., Fetcho, R.N., Huang, B.S., Huynh, T.N., Witztum, J., Shaver, D.C., Rosenthal, D.L., Alway, E.J., et al. (2019). Sustained rescue of prefrontal circuit dysfunction by antidepressant-induced spine formation. Science *364*, eaat8078. https://doi.org/10.1126/science.aat8078.
41. Lebow, M.A., and Chen, A. (2016). Overshadowed by the amygdala: the bed nucleus of the stria terminalis emerges as key to psychiatric d isorders. Mol. Psychiatr. *21*, 450–463. https://doi.org/10.1038/mp.2016.1.
42. Fitzgerald, P.B., Segrave, R., Richardson, K.E., Knox, L.A., Herring, S., Daskalakis, Z.J., and Bittar, R.G. (2018). A pilot study of bed nucleus of the stria terminalis deep brain stimulation in treatment-resistant de pression. Brain Stimul. *11*, 921–928. https://doi.org/10.1016/j.brs.2018.04.013.
43. Salimando, G.J., Hyun, M., Boyt, K.M., and Winder, D.G. (2020). BNST GluN2D-Containing NMDA Receptors Influence Anxiety- and Depressive-like Behaviors and ModulateCe ll-Specific Excitatory/Inhibitory Synaptic Balance. J. Neurosci. *40*, 3949–3968. https://doi.org/10.1523/JNEUROSCI.0270-20.2020.
44. Yu, G., and Sharp, B.M. (2012). Nicotine modulates multiple regions in the limbic stress network regulating activation of hypophysiotrophic neurons in hypothalamic paraventricular nucleus. J. Neurochem. *122*, 628–640. https://doi.org/10.1111/j.1471-4159.2012.07785.x.
45. Radley, J.J., and Johnson, S.B. (2018). Anteroventral bed nuclei of the stria terminalis neurocircuitry: Towards an integration of HPA axis modulation with coping behaviors - Curt Richter Award Paper 2017. Psychoneuroendocrino *89*, 239–249.

https://doi.org/10.1016/j.psyneuen.2017.12.005.

46. Iwabuchi, S.J., Krishnadas, R., Li, C., Auer, D.P., Radua, J., and Palaniyappan, L. (2015). Localized connectivity in depression: a meta-analysis of resting state functional imaging studies. Neurosci. Biobehav. Rev. *51*, 77–86. https://doi.org/10.1016/j.neubiorev.2015.01.006.
47. Kadriu, B., Musazzi, L., Johnston, J.N., Kalynchuk, L.E., Caruncho, H.J., Popoli, M., and Zarate, C.A. (2021). Positive AMPA receptor modulation in the treatment of neuropsychiatric disorders: A long and winding road. Drug Discov. Today *26*, 2816–2838. https://doi.org/10.1016/j.drudis.2021.07.027.
48. Lu, J., Zhang, Z., Yin, X., Tang, Y., Ji, R., Chen, H., Guang, Y., Gong, X., He, Y., Zhou, W., et al. (2022). An entorhinal-visual cortical circuit regulates depression-like behaviors. Mol. Psychiatr. *27*, 3807–3820. https://doi.org/10.1038/s41380-022-01540-8.
49. Warden, M.R., Selimbeyoglu, A., Mirzabekov, J.J., Lo, M., Thompson, K.R., Kim, S.Y., Adhikari, A., Tye, K.M., Frank, L.M., and Deisseroth, K. (2012). A prefrontal cortex-brainstem neuronal projection that controls response to behavioural challenge. Nature *492*, 428–432. https://doi.org/10.1038/nature11617.
50. Proulx, C.D., Aronson, S., Milivojevic, D., Molina, C., Loi, A., Monk, B., Shabel, S.J., and Malinow, R. (2018). A neural pathway controlling motivation to exert effort. P natl acad sci USA *115*, 5792–5797. https://doi.org/10.1073/pnas.1801837115.
51. Covington, H.E., Lobo, M.K., Maze, I., Vialou, V., Hyman, J.M., Zaman, S., LaPlant, Q., Mouzon, E., Ghose, S., Tamminga, C.A., et al. (2010). Tamminga, et al., Antidepressant effect of optogenetic stimulation of the medial prefrontal cortex. J. Neurosci. *30*, 16082–16090. https://doi.org/10.1523/JNEUROSCI.1731-10.2010.
52. Yin, Y.Y., Wang, Y.H., Liu, W.G., Yao, J.Q., Yuan, J., Li, Z.H., Ran, Y.H., Zhang, L.M., and Li, Y.F. (2021). The role of the excitation:inhibition functional balance in the mPFC in the onset of antidepressants. Neuropharmacology *191*, 108573. https://doi.org/10.1016/j.neuropharm.2021.108573.
53. Cipriani, A., Furukawa, T.A., Salanti, G., Chaimani, A., Atkinson, L.Z., Ogawa, Y., Leucht, S., Ruhe, H.G., Turner, E.H., Higgins, J.P.T., et al. (2018). Comparative efficacy and acceptability of 21 antidepressant drugs for the acute treatment of adults with major depressive disorder: a systematic review and network meta-analysis. Lancet *391*, 1357–1366. https://doi.org/10.1016/S0140-6736(17)32802-7.
54. Pastor, V., and Medina, J.H. (2021). Medial prefrontal cortical control of reward- and aversion-based behavioral output: Bottom-up modulation. Eur. J. Neurosci. *53*, 3039–3062. https://doi.org/10.1111/ejn.15168.
55. Emmons, E.B., De Corte, B.J., Kim, Y., Parker, K.L., Matell, M.S., and Narayanan, N.S. (2017). Rodent Medial Frontal Control of Temporal Processing in the Dorsomedial Striatum. J. Neurosci. *37*, 8718–8733. https://doi.org/10.1523/JNEUROSCI.1376-17.2017.
56. Suh, Y.H., Chang, K., and Roche, K.W. (2018). Metabotropic glutamate receptor trafficking. Mol. Cell. Neurosci. *91*, 10–24. https://doi.org/10.1016/j.mcn.2018.03.014.
57. Selvakumar, B., Jenkins, M.A., Hussain, N.K., Huganir, R.L., Traynelis, S.F., and Snyder, S.H. (2013). S-nitrosylation of AMPA receptor GluA1 regulates phosphorylation, single-channel conductance, and end ocytosis. Proc. Natl. Acad. Sci. USA *110*, 1077–1082. https://doi.org/10.1073/pnas.1221295110.
58. Gordillo-Salas, M., Pascual-Antón, R., Ren, J., Greer, J., and Adell, A. (2020). Antidepressant-Like Effects of CX717, a Positive Allosteric Modulator of AMPA Receptors. Mol. Neurobiol. *57*, 3498–3507. https://doi.org/10.1007/s12035-020-01954-x.
59. Aleksandrova, L.R., and Phillips, A.G. (2021). Neuroplasticity as a convergent mechanism of ketamine and classical psychedelics. Trends Pharmacol. Sci. *42*, 929–942. https://doi.org/10.1016/j.tips.2021.08.003.
60. Lewis, G. (2018). Transcranial magnetic stimulation for depression. Lancet *391*, 1639–1640. https://doi.org/10.1016/S0140-6736(18)30863-8.
61. Mutz, J., Vipulananthan, V., Carter, B., Hurlemann, R., Fu, C.H.Y., and Young, A.H. (2019). Comparative efficacy and acceptability of non-surgical brain stimulation for the acute treatment of major depressive episodes in adults: systematic review and network meta-analysis. Bmj *364*, l1079. https://doi.org/10.1136/bmj.l1079.
62. Fox, C.A., and McLoughlin, D.M. (2021). Speed of electroconvulsive therapy for depression: Effects of electrode placement. Acta Psychiatr. Scand. *143*, 444–452. https://doi.org/10.1111/acps.13286.
63. Sorinas, J., Grima, M.D., Ferrandez, J.M., and Fernandez, E. (2019). Identifying Suitable Brain Regions and Trial Size Segmentation for Positive/Negative Emotion Recognit ion. Int. J. Neural Syst. *29*, 1850044. https://doi.org/10.1142/S0129065718500442.
64. Zhong, H., Tong, L., Gu, N., Gao, F., Lu, Y., Xie, R.G., Liu, J., Li, X., Bergeron, R., Pomeranz, L.E., et al. (2017). Endocannabinoid signaling in hypothalamic circuits regulates arousal from general anesthesia in mice. J. Clin. Invest. *127*, 2295–2309. https://doi.org/10.1172/JCI91038.
65. Wang, M., Li, P., Li, Z., da Silva, B.S., Zheng, W., Xiang, Z., He, Y., Xu, T., Cordeiro, C., Deng, L., et al. (2023). Lateral septum adenosine A2A receptors control stress-induced depressive-like behaviors via signaling to the hypothalamus and habenula. Nat. Commun. *14*, 1880. https://doi.org/10.1038/s41467-023-37601-x.
66. Ji, Y.W., Shen, Z.L., Zhang, X., Zhang, K., Jia, T., Xu, X., Geng, H., Han, Y., Yin, C., Yang, J.J., et al. (2023). Plasticity in ventral pallidal cholinergic neuron-derived circuits contributes to comorbid chronic pain-like and depression-like behaviour in male mice. Nat. Commun. *14*, 2182. https://doi.org/10.1038/s41467-023-37968-x.

STAR★METHODS

KEY RESOURCES TABLE

REAGENT or RESOURCE	SOURCE	IDENTIFIER
Antibodies		
Rabbit anti-c-Fos mAb	Cell Signaling Technology	Cat#2250S
Mouse anti-CaMKIIα	Cell Signaling Technology	Cat#50049S
Rabbit anti-GAD1	Proteintech	Cat#10408-1-AP; RRID: AB_2107733
Guinea pig anti-c-Fos	Synaptic Systems	Cat#226004; RRID: AB_2619946
Alexa Fluor 405 donkey anti-Rabbit IgG (H + L)	Thermo Fisher Scientific	Cat#A48258; RRID: AB_2890547
Alexa Fluor 488 donkey anti-Rabbit IgG (H + L)	Thermo Fisher Scientific	Cat#A32790; RRID: AB_2762833
Alexa Fluor 488 donkey anti-Mouse IgG (H + L)	Thermo Fisher Scientific	Cat#A32766; RRID: AB_2762823
Alexa Fluor 594 goat anti-guinea pig IgG (H + L)	Thermo Fisher Scientific	Cat#A-11076; RRID: AB_2534120
Alexa Fluor 594 donkey anti-Rabbit IgG (H + L)	Thermo Fisher Scientific	Cat#A32754; RRID: AB_2762827
Alexa Fluor 594 donkey anti-Mouse IgG (H + L)	Thermo Fisher Scientific	Cat#A32744; RRID: AB_2762826
Bacterial and virus strains		
rAAV-Ef1α-DIO-mCherry-WPRE-pA，AAV 2/9，Retro	BrainVTA	Cat#PT-0013
rAAV-Ef1α-DIO-mCherry-WPRE-pA，AAV 2/9	BrainVTA	Cat#PT-0013
rAAV-Ef1α-DIO-EGFP-WPRE-pA，AAV 2/9	BrainVTA	Cat#PT-0795
rAAV-Ef1α-DIO-hChR2(H134R)-mCherry-WPRE-pA， AAV 2/9	BrainVTA	Cat#PT-0002
rAAV-Ef1α-DIO-eNpHR3.0-mCherry-WPRE-pA，AAV 2/9	BrainVTA	Cat#PT-0007
rAAV-Ef1α-DIO-hM3D(Gq)-mCherry-WPRE-pA，AAV 2/9	BrainVTA	Cat#PT-0042
rAAV-Ef1α-DIO-hM4D(Gi)-mCherry-WPRE-pA，AAV 2/9	BrainVTA	Cat#PT-0043
rAAV-CaMKIIα-Cre-WPRE-pA，AAV 2/9，Retro	BrainVTA	Cat#PT-0220
rAAV-Ef1α-DIO-GCaMp6s-WPRE-pA，AAV 2/9	BrainVTA	Cat#PT-0071
rAAV-Ef1α-fDIO-EGFP-WPRE-hGH-pA	BrainVTA	Cat#PT-1047
rAAV-CAG-DIO-WGA-FLP-WPRE-hGH-pA	BrainVTA	Cat#PT-0557
Chemicals, peptides, and recombinant proteins		
CNO	ApexBio	Cat# A3317
Tamoxifen	Sigma-Aldrich	Cat#10540-29-1
Ketamine	Shanghai Pharma	N/A
Experimental models: Organisms/strains		
Mouse: C57	Experimental Animal Center of Xuzhou Medical University	N/A
Mouse: Vglut1-iCreERT2	Zhong et al.	N/A
Mouse: Vgat-Cre: STOCK Slc32a1$^{tm2(cre)Lowl}$/J	The Jackson Laboratory	JAX: 016962
Software and algorithms		
FV10-ASW	Olympus	N/A
MATLAB	MathWorks	N/A
GraphPad Prism 8	GraphPad	N/A
Other		
Optical fibers	inper	N/A

RESOURCE AVAILABILITY

Lead contact

Further information and requests for resources and reagents should be directed to and will be fulfilled by the lead contact, Yong-mei Zhang (zhangym700@163.com).

Materials availability

This study did not generate new unique reagents.

Data and code availability

- Data reported in this paper will be shared by the lead contact upon request.
- This paper does not report original code.
- Any additional information required to reanalyze the data reported in this paper is available from the lead contact upon request.

EXPERIMENTAL MODEL AND STUDY PARTICIPANT DETAILS

Animals

Male wildtype C57BL/6J mice (Experimental Animal Center of Xuzhou Medical University), Vglut1-iCreERT2 mice,[64] and Vgat-Cre mice (Jackson Laboratory) were used in the experiments. Vglut1-iCreERT2 mice were used in experiments requiring labeling or manipulation of glutamatergic neurons, whereas Vgat-Cre mice were used for recording the activity of GABAergic neurons. 423 mice were used in our experiments. All mice (8–12 weeks, 22–26 g) were housed in standard laboratory conditions (12 h light/12 h dark cycle, temperature of 23–25°C, humidity of 60–70%, food and water *ad libitum*). Mice were group-housed at random (5–6 per cage) and subjected to tests during the light phase of the cycle (7 a.m.–7 p.m.). The experimenters were blind to group allocation. The experiments were conducted in accordance with the National Institutes of Health Guidelines for the Care and Use of Laboratory Animals and were approved by the Ethics Committee on Experimental Animals of Xuzhou Medical University. Efforts were made to minimize animal suffering and the number of animals used.

Tamoxifen administration for Vglut1-iCreERT2 mice

Vglut1-iCreERT2 mice contain a mutated version of the ligand-binding region of the estrogen receptor (ERT) expressed as a fusion protein with Cre recombinase. iCreERT2 is inactive in the cytoplasm in the absence of tamoxifen. When tamoxifen is administrated, its metabolites bind to ERT and permit iCreERT2 to enter the nucleus to exert Cre recombinase activity. Tamoxifen (Sigma-Aldrich, USA) was dissolved in sterile corn oil to make a working stock of 20 mg/ml. The procedure required 12 h of shaking at 37°C and then storage at 4°C, both in the dark. Two to three weeks after virus injections, mice were injected with tamoxifen solution (80 mg/kg) intraperitoneally for 5 consecutive days, with the experiments conducted subsequently.

Establishment of a depression model in mice

Mice were exposed to chronic restraint stress by placing them in a custom-made device for 2 h (10 a.m.–12 p.m.) per day for 10 consecutive days. The device consisted of cylindrical hollow metal mesh (8 cm in length and 2.5 cm in diameter) with an acrylic baffle that allowed satisfactory ventilation. These mice were also housed singly during the 10-day period, unlike control mice, which were always housed in groups of five or six. During the experiments, we ensured that all mice remained healthy and were protected from potential hazards.

METHOD DETAILS

Open-field test

Given that changes in general locomotor activity can skew the results of the tail-suspension and the forced-swim tests, we conducted an open-field test to assess whether any such changes occurred. The device used for the open-field test was a square arena (50 cm × 50 cm × 50 cm) consisting of a white bottom and four black walls, evenly illuminated under low light conditions. Prior to the test, mice were transferred from the housing room to the procedure room 1 h in advance. In each experiment, the mouse was gently placed in the center of the arena, facing one of the walls. Five minutes were allotted for the test, during which mice were allowed to move freely. Following each test, we wiped the arena with 75% ethanol and let it air dry to prevent the scent of the previous mouse affecting the behavior of subsequent mice. The total distance traveled was analyzed as a measure of animal locomotion with ANY-maze software.

Tail-suspension test

The tail-suspension test is intended to detect changes in effortful stress coping. Mice were habituated to the environment (a brightly lit room) for 1 h before the test. The apparatus for testing was a horizontal metal crossbar with a white wire hanging from it. The distal third of the mouse's tail was attached to the white wire with medical tape, so that the mouse was suspended upside down with its head approximately 20 cm above the ground. To prevent the mouse from climbing its own tail, we cut the tip off a 1 ml gun to 5 cm and used it to sheath the tail. The duration of mouse activity and inactivity was measured over 5 min. The surface below the apparatus was cleaned with 75% ethanol

between each trial. Time spent immobile was recorded manually: immobility was defined as when the mouse was either completely immobile in the air or had only small swing movements of the forelimbs. The proportion of time spent immobile during the 5-min test period was used to indicate depression-like behavior.

Forced-swim test

The forced-swim test was conducted to assess despair behavior. The testing room was maintained at a temperature of 25°C, and the mice were habituated to the room for 1 h in advance of the experiment. Mice were placed in a Plexiglas cylinder (30 cm tall; 15 cm in diameter) containing water at 23 ± 1°C to a depth of 20 cm. Mice remained in the water for 6 min without being able to escape. An experienced observer recorded immobility events as an analog of a depressed state during the test. Immobility was defined as floating motionless in the water or with slight limb movement to maintain balance. We replaced the water between each test in order to avoid odor interference. Mice were placed on a heating pad after the test to minimize any harm.

Sucrose-preference test

The sucrose-preference test was performed to evaluate hedonistic behavior in the mice. It incorporated a two-bottle choice paradigm. Mice were habituated to drinking from two plastic bottles equipped with ball-point sippers for two days, followed by a fasting day. On the first habituation day, two bottles of 1% sucrose solution were provided. On the second habituation day, one bottle of 1% sucrose solution and one bottle of pure water were provided and the positions of the two bottles were switched after 12 h. On the next day, mice were denied water and food for 24 hours, before being tested. During the test, each mouse was separated into an individual cage and supplied with two bottles. The bottles were filled with 1% sucrose solution or pure water, and we switched the bottle positions half-way through the 2-h test. The amount consumed from each bottle during the test was recorded and then transformed into a sucrose percentage: [weight of sucrose consumed / weight of sucrose and pure water consumed] × 100%.

Immunohistochemistry

Mice were anesthetized with intraperitoneal injection of 1% pentobarbital (40 mg/kg) and perfused transcardially with 0.9% sodium chloride (30 ml) and 4% paraformaldehyde (20 ml). The brains were extracted and immediately post-fixed in 4% paraformaldehyde for 10 h, then embedded in 30% sucrose solution for 48 h at 4°C. The brains were sliced into 30-μm free-floating coronal sections on a frozen-section microtome (CM1800; Leica Microsystems, Wetzlar, Germany). According to the mouse brain atlas in stereotaxic coordinates (third edition), the sections 1.98 mm to 1.78 mm from bregma were separated for immunostaining. Bregma +1.98 was used as a landmark. To prepare for immunofluorescence staining, the sections were rinsed in phosphate-buffered saline (PBS, pH 7.4) for 30 min (3 times for 10 min each), and subsequently blocked for 1 h with a PBS solution containing 5% donkey serum albumin and 0.25% Triton X-100. Afterwards, sections were incubated with primary antibodies at 4°C for 24–48 h depending on the experimental requirements. Upon completion, the sections were transferred to ambient temperature and gently rewarmed for 30 min, rinsed with PBS for 30 min (3 times for 10 min each), and then tagged with secondary antibodies for 2 h. Lastly, the sections were rinsed with PBS again for 30 min (3 times for 10 min each). Sections were mounted on glass slides, and then cover-slipped with an anti-fluorescence quencher containing 4′,6-diamidino-2-phenylindole (DAPI). The finished samples were stored in the dark at −20°C until they were imaged with a confocal laser microscope (FV1000, Olympus, Tokyo, Japan). Fluorescence images were captured under a 10× or 20× objective and then processed and counted with the NIH ImageJ software.

Stereotactic surgery

Mice were anesthetized with 1% sodium pentobarbital (40 mg/kg) and mounted on a stereotaxic apparatus (RWD, Shenzhen, China). Ophthalmic ointment was applied to prevent dehydration. To expose the cranium, the scalp was disinfected and a lengthwise incision was performed. Then we removed the periosteum with 3% hydrogen peroxide and washed the residue off with normal saline. Microinjection of virus was accomplished via a syringe (Hamilton, USA) after drilling holes in the skill for virus delivery. Virus was injected at the targeted site at a flow rate of 60 nl/min. To target the PrL, the coordinates were AP: 1.98 mm; ML: ± 0.25 mm; DV: −2.2 mm. To target the avBNST, the coordinates were AP: 0.45 mm; ML: ± 1.1 mm; DV: −4.7 mm. We left the needle at the target site for 10 min after injection to allow for diffusion of the virus and the removed it from the brain slowly over a three-minute period. According to the experimental needs, optical fibers or catheters were subsequently implanted in the corresponding location and secured with dental cement. Afterwards, the incision was sutured and the mouse placed on a heating blanket, then transferred to a cage for further recovery once awake. Mice did not exhibit noticeable behavioral changes during the postoperative period; in particular, they did not appear to have any visual impairments.

Chemogenetics

rAAV-Ef1α-DIO-hM3D(Gq)-mCherry-WPRE-hGH-pA and rAAV-Ef1α-DIO-hM4D(Gi)-mCherry-WPRE-hGH-pA were infused into the PrL of Vglut1-iCreERT2 mice for selective manipulation of glutamatergic neurons. The control virus was rAAV-Ef1α-DIO-mCherry-WPRE-hGH-pA. Three weeks were allowed for viral expression. Clozapine N-oxide (CNO, BrainVTA, China) was administered to activate the designer (Gi/Gq-coupled) receptors exclusively activated by designer drugs (DREADDs). In order to determine the overall effect of activation of PrL glutamatergic neurons, CNO (1 M) was injected intraperitoneally at a dose of 3 mg/kg. However, for modulation of the avBNST-projecting

glutamatergic neurons in the PrL, catheters were implanted above the avBNST and 150 nl CNO (1 mM) was delivered via the catheter. Subsequent tests were performed 30 min after CNO treatment.

Optogenetics

rAAV-Ef1α-DIO-hChR2(H134R)-mCherry-WPRE-pA and rAAV-Ef1α-DIO-eNpHR3.0-mCherry-WPRE-pA were injected into the PrL. For examination of specific circuit effects on depression-like behaviors, an optical fiber was implanted 200 μm above the avBNST to activate or inhibit the $PrL^{Glu} \rightarrow avBNST^{GABA}$ glutamatergic terminals. Laser power measured at the tip of the optical fiber was 4 mW for the blue laser refer to previous studies.[65,66] Mice were subjected to constant photostimulation or photoinhibition during the open-field, tail-suspension, and forced-swim tests. In the sucrose-preference test, however, mice received photostimulation/photoinhibition only during the first 30 min (two-minute light stimulation episodes were delivered with 2 min intervals for 30 min) of the 2-h period to minimize tissue damage from prolonged light exposure.

Fiber photometry

Real-time Ca^{2+} transients were assessed via fiber photometry (ThinkerTech, Nanjing, China) to determine changes in neuronal activity. Depending on the experiment, we microinjected 150 nl of rAAV-CaMKIIα-CRE-WPRE-hGH-pA (retro) into the avBNST and 200 nl of rAAV-Ef1α--DIO-GCaMp6s-WPRE-hGH-pA into the PrL of C57BL/6J mice, or 200 nl of rAAV-Ef1α-DIO-GCaMp6s-WPRE-hGH-pA into the PrL of Vglut1-iCreERT2 mice, or 150 nl of rAAV-Ef1α-DIO-GCaMp6s-WPRE-hGH-pA into the avBNST of Vgat-Cre mice. An optical fiber (230 μm OD, 0.37 NA, Inper, Hangzhou, China) was implanted over the region injected with GCaMp6s virus and fixed in place with dental cement. Three weeks after viral expression, the calcium activity of the target neurons was monitored. Fiber photometry recordings were performed on awake mice that were simultaneously undergoing the tail-suspension test. Struggling behavior was quantified by area under the calcium fluorescence intensity curve. It was recorded manually by the same experienced experimental observer. Not every slight movement in the test was considered as struggling behavior, only the movement of both head and limbs of the mice was considered as struggling behavior and the pendulum-like activity of the mice was considered as a desperate state of the animal due to the inertia of the movement. If a struggling behavior occurred during the window period of another, we did not record this behavior as the calcium fluorescence intensity did not drop to baseline levels at this time. Fluorescence signals were obtained by reflecting a laser beam from a laser tube (473 nm) onto a dichroic mirror, focusing it with a 10× lens, and then coupling it to an optical commutator. Light was guided from the implanted fiber to the commutator by a 2-m optical fiber. To minimize photobleaching, the power intensity at the fiber tip was set to between 0.02 and 0.04 mW and the sampling frequency was 100 Hz. The calcium signals were acquired with data-acquisition software (ThinkerTech, Nanjing, China) and the onset of struggling during the tail-suspension test was recorded manually. Raw signals were analyzed and processed with a Matlab program developed by Thinkertech. For each trial, the fluorescence variation was calculated as the z-score = $(F-F0)/\sigma F$, where F represents the test signal and F0 and σF are the mean and standard deviation of the basal signal, respectively. The z-score values were segmented according to the onset of the struggle events and averaged across trials. For this calculation, the baseline was considered to be the average signal from −3 s to −1 s. The area under the curve (AUC) for the 5 s after the onset of a struggle event was calculated as a metric to quantify the calcium fluorescence intensity and was used in subsequent statistical analyses.

QUANTIFICATION AND STATISTICAL ANALYSIS

Statistical analyses were conducted in Prism v.8.0 (GraphPad). Two-tailed Student's *t*-tests were used for comparisons between two independent groups. For comparisons of more than two independent groups, we used a one-way analysis of variance (ANOVA) with Bonferroni post hoc tests. The two-way ANOVA was used for two-factorial designs, followed by Bonferroni's post hoc test to further test differences between groups. A mixed-effects ANOVA was used to perform linear mixed-effects modeling with multiple measurements, followed by Bonferroni post hoc tests. Data are presented as the mean ± standard error of the mean (SEM). Statistical significance was defined as a p value less than 0.05.